Dalton Transactions

ROYAL SOCIETY OF CHEMISTRY

PAPER

View Article Online
View Journal | View Issue

Check for updates

Cite this: *Dalton Trans.*, 2023, **52**, 5780

Selecting optimal R_6TX_2 intermetallics (R = Gd, Tb, Dy; T = Mn, Fe, Co, Ni; X = Sb, Te) for magnetic refrigeration†

A. Herrero, *[a] I. R. Aseguinolaza,[a] A. Oleaga, [a] A. J. Garcia-Adeva, [a] E. Apiñaniz,[a] A. V. Garshev,[b] V. O. Yapaskurt[c] and A. V. Morozkin[b]

Received 23rd January 2023,
Accepted 20th March 2023

DOI: 10.1039/d3dt00223c

rsc.li/dalton

A complete experimental study of the physical properties playing a relevant role in the magnetic refrigeration application (structural, magnetic, magnetocaloric and thermal) has been performed over nine selected Fe_2P-type R_6TX_2 (R = Gd, Tb, Dy; T = Mn, Fe, Co, Ni; X = Sb, Te) intermetallic compounds, to work close to room temperature. Two magnetic phase transitions are observed for these materials: a paramagnetic to ferromagnetic transition in the range of 182–282 K and a spin reorientation transition in the range of 26–76 K. As a consequence, two peaks related to a direct magnetocaloric effect (DMCE) appear with the magnetic entropy change, generating a wide table-like plateau region in between both peaks, which is required to improve the efficiency of refrigerators following an Ericsson cycle. The highest magnetic entropy peak value for $\mu_0\Delta H$ = 5 T is found for $Tb_2Dy_4FeSb_2$, with 7.72 J kg^{-1} K^{-1} around 182 K. For the same applied field the other compounds show moderate values around room temperature (2.88–4.53 J kg^{-1} K^{-1}). However, the superposition of the two peaks results in huge refrigerant capacity values, up to RC_{FWHM}(5 T) = 1103.04 J kg^{-1} in the case of $Tb_2Dy_4FeSb_2$. The thermal diffusivity, thermal effusivity, thermal conductivity and specific heat capacity have been measured at room temperature, and the temperature dependence of the former has been obtained around the relevant magnetic phase transition region, with values in the range of 1.3–2.3 mm^2 s^{-1}, which are good for magnetic refrigerators at high working frequencies. The study is completed with a rigorous critical behavior analysis of the second order PM–FM transition. The critical exponent γ points to long range order interactions, in general, while β values are in the range of 0.59–0.90, indicating a deviation from theoretical models as a reflection of the magnetic complexity in these compounds. The critical exponents have been used to confirm the scaling relations of magnetocaloric properties, and the scaling of refrigerant capacity (RC) values in materials exhibiting two magnetic phase transitions is addressed, concluding that for a correct scaling of RC the magnetic entropy change peak must be considered symmetric. The role of each atom in the properties of the compounds is discussed.

1. Introduction

Magnetic refrigeration has emerged as one of our greatest technological allies in the efforts to avoid the worst consequences arising from climate change. This refrigeration system intends to substitute the actual gas compression-expansion based technologies.[1–3] The main advantages of magnetic refrigeration are the greater expected efficiency and the lack of ozone depletion or greenhouse effect related substances for their functioning, which make this a more environmentally friendly refrigeration system.[3] As a consequence of the huge technological interest in these devices, research on different magnetocaloric materials has been increasing in the last few decades.

The great magnetic moment of rare-earth elements as well as the complex magnetic structures and interactions arising from their combination with other metals is what makes rare-earth containing intermetallics so interesting. In recent years a growing amount of effort has been dedicated to the study of binary, ternary or even quaternary intermetallic compounds,

[a]*Departamento de Física Aplicada, Escuela de Ingeniería de Bilbao, Universidad del País Vasco UPV/EHU, Plaza Torres Quevedo 1, 48013 Bilbao, Spain. E-mail: aritz.herrero@ehu.eus*
[b]*Department of Chemistry, Moscow State University, Lenisnkie Gory, House 1, Building 3, Moscow, GSP-2, 119991, Russia*
[c]*Department of Petrology, Geological Faculty, Moscow State University, Leninskie Gory, Moscow, 119991, Russia*

† Electronic supplementary information (ESI) available. See DOI: https://doi.org/10.1039/d3dt00223c

such as Laves phases (AB_2 composition),[4–6] the RTX (R = rare-earth, T = transition metal, X = p-block element) family,[7,8] R_2T_2X,[9] R_3(Co, Ni)[10,11] or $Gd_5(Si, Ge)_4$ [1,12] families, to mention some of them. Other kinds of compounds such as manganites, Heusler alloys or high entropy alloys (HEA) are also being exhaustively studied.[13–18]

The applicability of magnetocaloric materials extends to the food industry, electronic devices, the space industry, cryogenic refrigeration and even medicine;[9,19–24] however, most efforts have been focused on domestic refrigeration in the room temperature region.[2,15]

Finding desirable physical properties for an ideal magnetocaloric material is one of the most searched goals. This is not a trivial task since many factors must be taken into account. The magnetocaloric effect is usually evaluated by the magnetic entropy change (ΔS_M), which is obtained from magnetic measurements through the well-known Maxwell relation.[1] Special attention must be paid to the nature and critical temperature of the magnetic phase transition. The maximum value of $|\Delta S_M|$ is obtained at the critical temperature (T_C) of the magnetic transition; therefore, T_C must be close to the working temperature. Furthermore, the order of magnetic phase transition also has an effect on the magnetocaloric properties. First order transitions usually show higher but sharper peaks with the magnetic entropy change, while second order magnetic phase transitions show lower but wider peaks. From the point of view of their application, high values of magnetocaloric variables over a wide temperature range are required, but without presenting magnetic or thermal hysteresis, typical of first order transitions, since this limits the applicability of the material in a refrigeration cycle.[25,26] This is why scientific research is mainly focused on magnetic materials exhibiting second order magnetic phase transitions or first order magnetic phase transitions with a small hysteresis.[1,27] The range of temperatures for which the magnetic entropy change is kept high is also relevant, and this defines the working temperature range and is usually characterized by the refrigerant capacity RC. One of the main research lines is to improve the performance of materials exhibiting second order magnetic phase transitions by playing with their stoichiometry in order to obtain a table-like magnetocaloric effect over a wide temperature range. Materials exhibting a constant value of the magnetic entropy change enhance the performance of an ideal Ericsson refrigeration cycle, which consists of two isothermal and two isofield processes.[1] Different approaches can be considered in order to achieve this table-like behavior, creating a multilayer system with materials showing close by transitions,[8,9,28] or finding a single material with several magnetic transitions. The second approach is the one considered in this work.

Regarding the application of magnetocaloric materials as refrigerants, the magnetic and magnetocaloric properties must be accompanied by good thermal properties. The purpose of these materials is to work under a thermodynamic cycle and therefore to exchange heat. In this context, materials with high thermal diffusivity values, which allow a faster heat exchange and higher working frequencies of the magnetocaloric refrigerator, are desired. In this work we focus our attention on the high resolution measurement of thermal diffusivity around the Curie temperature of each compound.

An understanding as profound as possible of the fundamental, magnetic, magnetocaloric and thermal properties that make a material a good magnetocaloric refrigerant is required. The purpose of this work is to explore the most relevant physical properties of some members of the general R_6TX_2 intermetallic family, in particular, $Gd_3Tb_3FeSbTe$, $Tb_2Dy_4FeSb_2$, $Tb_2Dy_4Fe_{0.75}Mn_{0.25}Sb_2$, $Gd_2Dy_4Fe_{0.75}Mn_{0.25}Sb_2$, $Gd_2Tb_4Fe_{0.75}Mn_{0.25}SbTe$, $Tb_6Fe_{0.75}Mn_{0.25}SbTe$, $Tb_6Co_{0.75}Mn_{0.25}SbTe$, $Tb_6Ni_{0.75}Mn_{0.25}SbTe$ and $Tb_6Ni_{0.5}Mn_{0.5}SbTe$ compounds. The samples presented in this work have been selected based on our previous research on $Ho_6(Fe,Mn)Bi_2$, $(Gd,Tb)_6(Fe,Mn)Bi_2$ and $Dy_6(Fe,Mn)X_2$ families.[29–31] Sb and Te have been selected as the X elements in order to increase the magnetocaloric effect, as was observed in previous studies.[31] The combination of Tb, Gd and Dy is also expected to improve the magnetocaloric properties and to place the critical temperature (T_C) closer to room temperature. Finally, Mn is also introduced into some compounds to further increase T_C, as this has been proved to be the case in the R_6TX_2 intermetallic family.[29–31] Therefore, these specific compositions, which have not been studied before, are expected to show a relevant table-like magnetocaloric effect with the Curie temperature close to room temperature and lower temperature spin reorientation transition. The effect of Co and Ni on the properties of these materials will also be discussed.

With the goal of gaining a deeper understanding of the highly tuneable R_6TX_2 family, which will enable the selection of optimum compositions for magnetic refrigeration, this study presents a discussion on the magnetic and thermal properties of nine selected compounds as well as the evaluation of their potential to be used as magnetic refrigerants. The analysis of the peculiar critical behavior of their second order ferromagnetic to paramagnetic phase transition will also be addressed. We will focus for the first time on the effect of the symmetry breaking of the magnetic entropy change peak at T_C due to the lower temperature transition, and discuss how to appropriately apply the scaling laws in this case.

2. Samples and experimental techniques

$Gd_3Tb_3FeSbTe$, $Tb_2Dy_4FeSb_2$, $Tb_2Dy_4Fe_{0.75}Mn_{0.25}Sb_2$, $Gd_2Dy_4Fe_{0.75}Mn_{0.25}Sb_2$, $Gd_2Tb_4Fe_{0.75}Mn_{0.25}SbTe$, $Tb_6Fe_{0.75}Mn_{0.25}SbTe$, $Tb_6Co_{0.75}Mn_{0.25}SbTe$, $Tb_6Ni_{0.75}Mn_{0.25}SbTe$ and $Tb_6Ni_{0.5}Mn_{0.5}SbTe$ alloys with a total mass of 2.5 g were prepared by arc-melting in an electric arc furnace (90 V, 150 A) under an argon atmosphere (99.992 vol%) using a non-consumable tungsten electrode and on a water-cooled copper hearth. Pieces of gadolinium, terbium, dysprosium (99.9 wt%), iron, manganese (99.95 wt%), tellurium and antimony (purity 99.99 wt%) with some surplus for dysprosium (0.05 g), manganese (0.015 g),

tellurium (0.05 g), and antimony (0.02 g) were used as starting components. A titanium button was used as a getter during arc-melting and the alloys were remelted three times. The arc-melted samples were wrapped into a nickel foil and sealed in silica ampoules, evacuated and backfilled with argon to 0.3 atm at room temperature. The samples were annealed at 1070 K (±2 K) for 300 hours, and then quenched in an ice-water bath.

Phase analysis of the alloys was carried out using X-ray diffraction and energy dispersive X-ray spectroscopy (EDS) microprobe elemental analysis. The powder X-ray diffraction (PXRD) data were obtained using a Rigaku D/MAX-2500 diffractometer (CuKα, 2θ values of 10–80° and 5–120°, 0.02° step, Imax/Ibgr ~50–90). An INCA-energy-350 X-ray EDS spectrometer (Oxford Instruments) with a Jeol JSM-6480LV scanning electron microscope (SEM) (20 kV accelerating voltage, 0.7 nA beam current, 50 μm beam diameter and ~10 nm microprobe size) was employed to perform quantitative elemental analysis. Signals averaged over three points per phase gave estimated standard deviations of 0.5 at% for Gd, Tb, and Dy (measured by L-series lines), 1 at% for Mn and Fe and 0.6 at% for Sb, Bi and Te (measured by K-series lines).

The unit cell data were derived from powder X-ray data using the Rietan-program[32] in the isotropic approximation at room temperature.

Magnetic measurements were performed using a VSM (Vibrating Sample Magnetometer) module with a PPMS (Physical Properties Measurement System) by Quantum Design. For each sample, Zero-Field Cooled (ZFC) and Field Cooled (FC) magnetization (M) measurements were performed as a function of temperature. Magnetization isotherms as a function of an externally applied magnetic field were also collected from 2 K to temperatures well above the Curie temperature corresponding to each sample. Special attention was paid to the region of magnetic phase transition, where a step of ΔT = 1 K between consecutive isotherms was used. Except for $Gd_2Tb_4Fe_{0.75}Mn_{0.25}SbTe$, for which isotherm magnetization measurements were performed up to 7 T, the maximum applied magnetic field was 8 T.

In order to correctly evaluate the critical behavior and magnetocaloric effect, the demagnetization effect was taken into account.[33] To this end, the internal field (H_i), obtained from $H_i = H_a - NM$ (N being the demagnetization factor), was used to perform the calculations, instead of the applied field. The demagnetization factor was obtained from the Hopkinson or principal maximum of the ac magnetic susceptibility,[34,35] which was measured on an AC measurement system in the same PPMS. The ac susceptibility data as a function of temperature were also used to precisely locate the transition temperatures. In order to simplify the notation, H will be used to denote the internal field (H_i) in the rest of the work.

The thermal properties of the materials were measured using a high-resolution ac photopyroelectric calorimeter (PPE), in its back detection configuration for thermal diffusivity measurements[36] and in its front detection configuration for thermal effusivity measurements.[37]

3. Experimental results and discussion

3.1. Structural data and phase analysis

The X-ray powder and EDS analyses (see ESI Fig. 1s†) showed that novel and $\{Gd\text{-}Dy\}_6FeTe_2$-, $\{Tb, Dy\}_6FeSb_2$- and $Tb_6\{Co, Ni\}Te_2$-based[38] $Gd_3Tb_3FeSbTe$, $Tb_2Dy_4FeSb_2$, $Tb_2Dy_4Fe_{0.75}Mn_{0.25}Sb_2$, $Gd_2Dy_4Fe_{0.75}Mn_{0.25}Sb_2$, $Gd_2Tb_4Fe_{0.75}Mn_{0.25}SbTe$, $Tb_6Fe_{0.75}Mn_{0.25}SbTe$, $Tb_6Co_{0.75}Mn_{0.25}SbTe$, $Tb_6Ni_{0.75}Mn_{0.25}SbTe$ and $Tb_6Ni_{0.5}Mn_{0.5}SbTe$ quasiternary compounds/solid solutions crystallize in the Fe_2P-type structure (space group $P\bar{6}2m$, no. 189, $hP9$). The refined unit cell data and atomic positions are given in Table 1.

Ternary Fe_2P-type rare compounds exhibit mixed metal/semimetal types of bonds as they show a monotonic increase of unit cell parameters in accordance with the atomic radii of rare earth metals[39] ($\{Gd\text{-}Er\}_6FeTe_2$ tellurides[38] in ESI Fig. 2s-a and 2s-b†), while replacements of the transition metals and p-elements (Sb, Bi, and Te) are followed *via* a non-monotonic change of unit cell parameters with a decrease of transition metal atomic radii[39] in the 'Mn–Co–Ni–Fe' row and an increase

Table 1 Unit cell data of Fe_2P-type quasiternary compounds (space group $P\bar{6}2m$, N 189, $hP9$)

N	Compound	a (nm)	c (nm)	c/a	V (nm^3)	R_F (%)
1	$Gd_3Tb_3FeSbTe$ [a,b]	0.82712(2)	0.41051(1)	0.49631	0.24322	3.6
2	$Tb_2Dy_4FeSb_2$	0.81481(5)	0.41703(2)	0.51181	0.23978	4.0
3	$Tb_2Dy_4Fe_{0.75}Mn_{0.25}Sb_2$	0.81478(6)	0.41866(3)	0.51383	0.24070	4.8
4	$Gd_2Dy_4Fe_{0.75}Mn_{0.25}Sb_2$	0.81646(6)	0.41991(3)	0.51431	0.24241	4.2
5	$Gd_2Tb_4Fe_{0.75}Mn_{0.25}SbTe$	0.82577(5)	0.41265(3)	0.49972	0.24369	5.6
6	$Tb_6Fe_{0.75}Mn_{0.25}SbTe$ [a]	0.82337(3)	0.41179(1)	0.50013	0.24177	4.2
7	$Tb_6Co_{0.75}Mn_{0.25}SbTe$	0.82547(6)	0.40704(2)	0.49310	0.24020	3.7
8	$Tb_6Ni_{0.75}Mn_{0.25}SbTe$	0.82927(7)	0.40245(3)	0.48531	0.23968	3.9
9	$Tb_6Ni_{0.5}Mn_{0.5}SbTe$	0.82840(7)	0.40553(3)	0.48953	0.24101	5.4

[a] Crystallographic data used with permission of JCPDS – International Centre for Diffraction Data (USA). [b] $Gd_3Tb_3FeSbTe$: $(Gd_{0.5}Tb_{0.5})1\ 3g$ [0.5962 (3), 0, 1/2], $(Gd_{0.5}Tb_{0.5})2\ 3f$ [0.2399(3), 0, 0], Fe $1b$ [0, 0, 1/2], and $(Sb_{0.5}Te_{0.5})\ 2c$ [1/3, 2/3, 0], and the atomic displacement parameters of all atoms $\beta_{11} = \beta_{22} = 0.004872$, $\beta_{12} = 0.002436$, $\beta_{33} = 0.014835$ ($\beta_{11} = B_{11}/(3a^2)$, $\beta_{12} = B_{22}/(6a^2)$, and $\beta_{33} = B_{33}/[2c]^2$).

of the atomic radii of the p-element[39] in the 'Te–Sb–Bi' row (as shown for $Ho_6\{Fe–Ni\}\{Sb, Bi, Te\}_2$ compounds in ESI Fig. 2s-c and 2s-d†).

Similar behavior of unit cell parameters was observed for the present quasiternary $Tb_2Dy_4FeSb_2$ which belongs to the continuous row of the $Tb_{6-x}Dy_xFeSb_2$ solid solution, for Dy_6FeSb_2- and $Tb_{6-x}Dy_xFeSb_2$-based $Gd_2Dy_4Fe_{0.75}Mn_{0.25}Sb_2$ and $Tb_2Dy_4Fe_{0.75}Mn_{0.25}Sb_2$, for $Tb_6FeSb_{2-x}Te_x$- and Gd_6FeTe_2-based $Gd_3Tb_3FeSbTe$, $Gd_2Tb_4Fe_{0.75}Mn_{0.25}SbTe$ and $Tb_6Fe_{0.75}Mn_{0.25}SbTe$ and for $Tb_6\{Co, Ni\}Te_2$-based $Tb_6\{Co, Ni\}_{0.75}Mn_{0.25}SbTe$ and $TbNi_{0.5}Mn_{0.5}SbTe$ (Fig. 1).

The substitution of rare earth metals is followed by a monotonic increase of unit cell parameters with an increase of rare earth atomic radii, like that observed for $Tb_2Dy_4FeSb_2$ (in comparison with Dy_6FeSb_2), for $Tb_2Dy_4Fe_{0.75}Mn_{0.25}Sb_2$ and $Gd_2Dy_4Fe_{0.75}Mn_{0.25}Sb_2$ and for $Tb_6Fe_{0.75}Mn_{0.25}SbTe$ and $Gd_2Tb_4Fe_{0.75}Mn_{0.25}SbTe$. The transformation of the unit cell in the '$Tb_6Fe_{0.75}Mn_{0.25}SbTe$-$Tb_6Co_{0.75}Mn_{0.25}SbTe$-$Tb_6Ni_{0.75}Mn_{0.25}SbTe' row with the substitution of transition metals corresponds to the one in the 'Ho_6MnTe_2–Ho_6FeTe_2–Ho_6CoTe_2–Ho_6NiTe_2' row. Meanwhile, the substitution of Te for Sb leads to the anisotropic transformation of the unit cell of initial tellurides as observed in this work for $Tb_6\{Fe, Co, Ni\}_{0.75}Mn_{0.25}SbTe$ and $Gd_3Tb_3FeSbTe$, like that observed for Ho-based ternary tellurides (see Fig. 1 and ESI Fig. 2s-c and 2s-d†).

Such transformation of the Fe_2P-type unit cell, the type of rare earth metal and magnetic catalysis of Mn–Mn–Mn chains[40] determine the magnetic ordering of Fe_2P-type quasiternary compounds. The synthesis of these multicomponent compounds may be followed *via* superstructure formation with the ordering of rare earth metal, transition metal and p-element sublattices which is an additional factor of magnetic ordering. However, this assumption was not confirmed by X-ray powder diffraction analysis.

Due to the diffusion synthesis method of the present Fe_2P-type quasiternary compounds, the alloys contain ~1–6 wt% of admixture phases with known magnetic properties[38] (ESI Table 1s†) whose influence is negligible or close to the ESD (Estimated Standard Deviation) of the resulting magnetic properties of the investigated compounds.

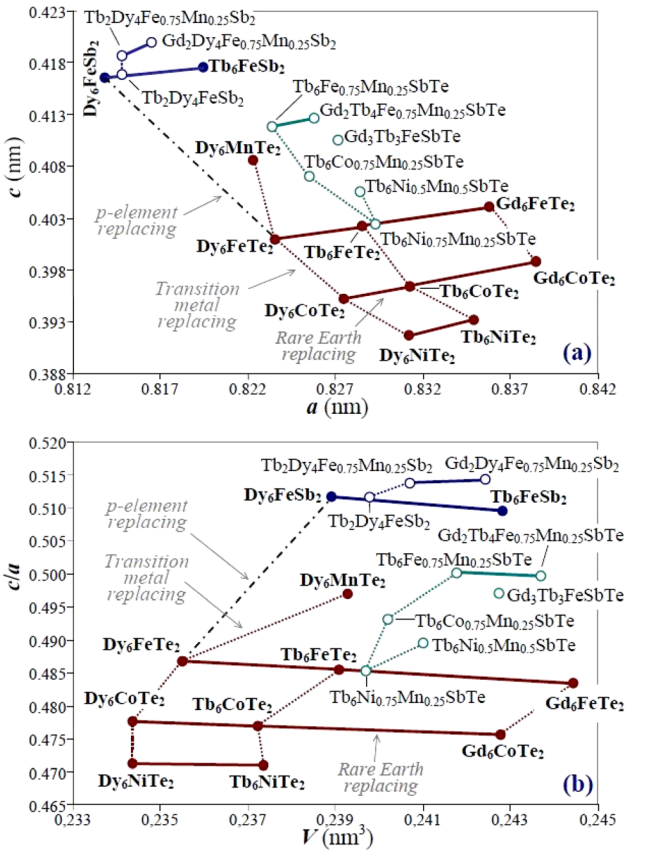

Fig. 1 Unit cell data of Fe_2P-type ternary antimonides (blue) and tellurides (brown) selected *via* boldface font and investigated quasiternary compounds/solid solutions (usual font): (a) cell parameter *c vs.* cell parameter *a* and (b) *c*/*a* ratio *vs.* unit cell volume *V*. Some replacements/substitutions of rare earth metals, transition metals and p-elements of the ternary (filled circles) and quasiternary (open cicles) compounds are marked in figures.

3.2. Magnetic characterization

The materials presented in this work are part of the larger R_6TX_2 intermetallic family, for which it is commonly accepted that the magnetic properties are solely ruled by the magnetic moments in the rare earth atoms. This has been suggested since no magnetic moment from the T element could be found after neutron diffraction experiments on other members of the same family.[40–46] The first step in order to characterize the magnetism of these samples is to precisely locate the transition temperatures in our compounds, as well as to observe and discuss the magnetic properties they exhibit. We performed Zero-Field Cooled (ZFC) and Field Cooled (FC) magnetization (M) measurements as a function of temperature. The ZFC and FC measurements are presented in the upper boxes (a) and (b) of Fig. 2. These curves clearly show the existence of paramagnetic to ferromagnetic transition at a higher temperature (T_C), which is followed by a second magnetic phase transition at a lower temperature (T_m). Both transitions are observed in all the compounds. The latter transition takes the compound from a collinear ferromagnetic state at higher temperatures to a complex non-collinear spin arrangement at lower temperatures, including canted ferromagnets, conical or spiral or simply antiferromagnetic, as has been observed by neutron diffraction techniques in other compounds of the R_6TX_2 family.[40,41,47] Fig. 2 shows a clear difference between FC (empty symbols) and ZFC (full symbols) measurements, pointing to high thermomagnetic irreversibility, typical of many ferromagnetic transitions. This behavior has already been observed in our previous studies on this family, with a greater effect on compounds containing Tb and Dy.[30,31] T_C and T_m are precisely indicated by the position of the peaks in the real part of ac susceptibility, as shown in the lower (c) and (d) graphs of Fig. 2. The PM–FM transition is located at 282 K for $Gd_2Tb_4Fe_{0.75}Mn_{0.25}SbTe$, 273 K for $Tb_6Fe_{0.75}Mn_{0.25}SbTe$, 271 K for $Tb_6Ni_{0.5}Mn_{0.5}SbTe$, 265 K for $Gd_2Dy_4Fe_{0.75}Mn_{0.25}Sb_2$, 260 K

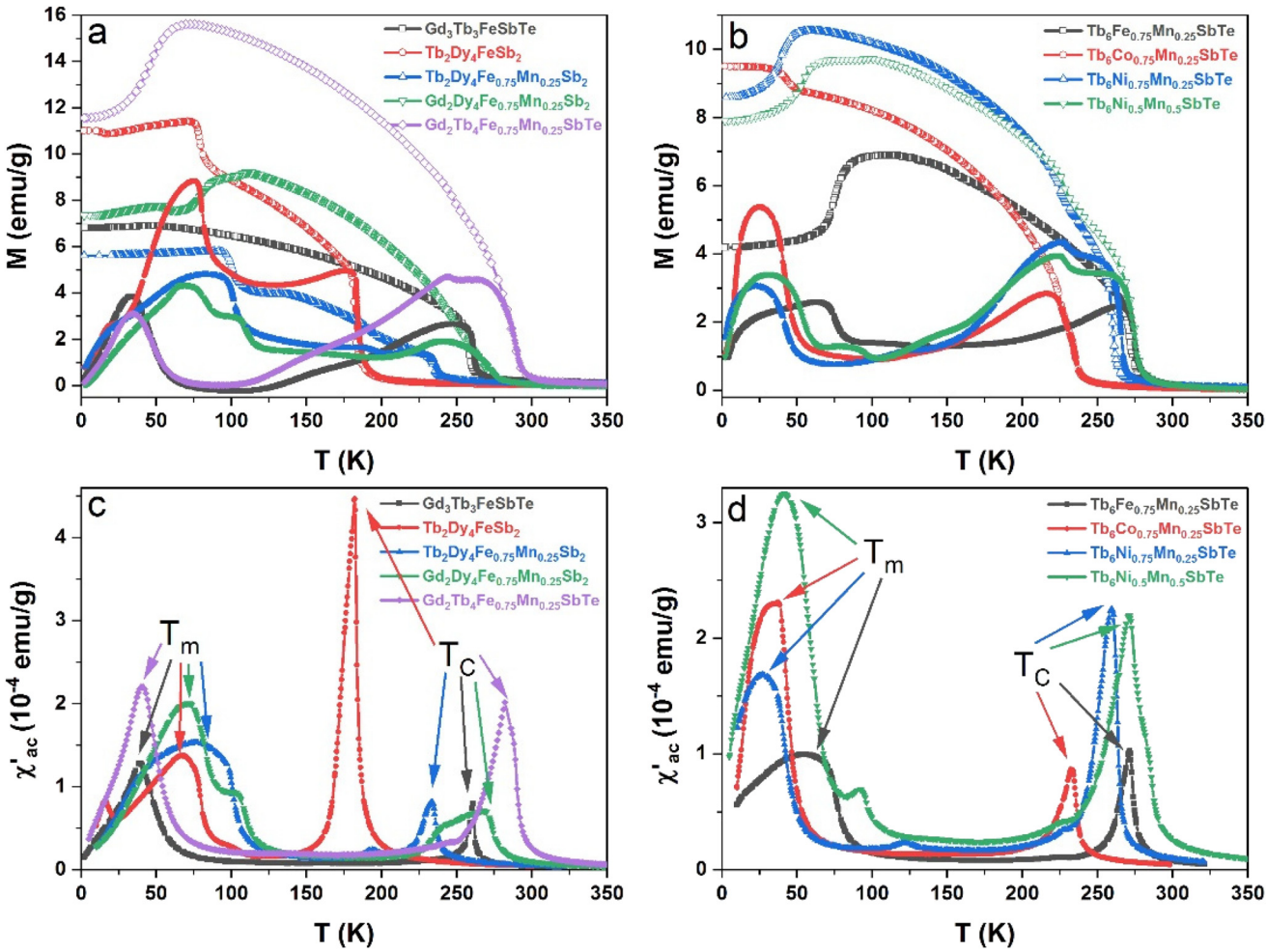

Fig. 2 Upper graphs (a) and (b): magnetic moment as a function of temperature in zero-field cooled (ZFC, open symbols) and field-cooled (FC, closed symbols) mode with applied field H = 100 Oe. Lower boxes (c) and (d): real part of the ac susceptibility at f = 100 Hz. T_C corresponds to the paramagnetic to ferromagnetic transitions, T_m to the spin reorientation ones. (a) and (c) for $Gd_3Tb_3FeSbTe$, $Tb_2Dy_4FeSb_2$, $Tb_2Dy_4Fe_{0.75}Mn_{0.25}Sb_2$, $Gd_2Dy_4Fe_{0.75}Mn_{0.25}Sb_2$, and $Gd_2Tb_4Fe_{0.75}Mn_{0.25}SbTe$; (b) and (d) for $Tb_6Fe_{0.75}Mn_{0.25}SbTe$, $Tb_6Co_{0.75}Mn_{0.25}SbTe$, $Tb_6Ni_{0.75}Mn_{0.25}SbTe$ and $Tb_6Ni_{0.5}Mn_{0.5}SbTe$.

for $Gd_3Tb_3FeSbTe$ and $Tb_6Ni_{0.75}Mn_{0.25}SbTe$, 233 K for $Tb_2Dy_4Fe_{0.75}Mn_{0.25}Sb_2$ and $Tb_6Co_{0.75}Mn_{0.25}SbTe$, and 182 K for $Tb_2Dy_4FeSb_2$, while T_m ranges from ~26 K in $Tb_6Ni_{0.75}Mn_{0.25}SbTe$ to ~76 K in $Tb_2Dy_4Fe_{0.75}Mn_{0.25}Sb_2$, and some of the latter peaks are wide and T_m is not precisely defined. As observed in previous works,[29–31] T_C increases as the Mn concentration increases, in both the cases of $Tb_2Dy_4FeSb_2$ to $Tb_2Dy_4Fe_{0.75}Mn_{0.25}Sb_2$ and in $Tb_6Ni_{0.75}Mn_{0.25}SbTe$ to $Tb_6Ni_{0.5}Mn_{0.5}SbTe$, although in the latter case the Curie temperature increase is smaller. The substitution of Tb by Gd in $(Tb,Gd)_2Dy_4Fe_{0.75}Mn_{0.25}Sb_2$ also increases the critical temperature. Finally, within the $Tb_6(Fe,Co,Ni)_{0.75}Mn_{0.25}SbTe$ series, T_C is higher in the Fe composition and lower in the Co composition, while the critical temperature for the Ni composition lies in between the previous values.

In this intermetallic family magnetic interactions are considered to take place between rare earth atoms and are described by an indirect 4f–4f RKKY (Ruderman–Kittel–Kasuya–Yosida) type interaction, where the d-band acts as a mediator. This interaction is very sensitive to the distance between atoms and to the different kinds of orbital hybridizations among the ions in the compound. This effect can be better observed by analysing the structural change induced by the substitution of elements (discussed in the previous section), and its role in determining the Curie temperature of each compound. Although many substitutions are taking place on these compounds, some general conclusions can be obtained. A bigger rare-earth atomic radius provokes the monotonic increase of the cell volume and c and a cell parameters, resulting in a higher PM–FM transition temperature. The distortion of the atomic cell by transition metal substitution is not so directly related to the T_C position, due to the difference induced in hybridization processes, which play a more relevant role. In Fig. 1 it can be observed how the c cell parameter and V cell volume always heavily increase when Mn is included in the compound, and this is probably due to its

higher atomic radius. In contrast, the *a* cell parameter slightly decreases with the Mn content. This cell distortion results in a severe T_C increase when Mn is present. The same behavior can be observed when Fe substitutes Co or Ni. However, although the substitution of Ni by Co is also followed by an increase of the *c* cell parameter and a decrease of the *a* cell parameter, the cell volume increases or decreases depending on the rare earth companion (Fig. 1(b)). The difference in hybridization when Fe is substituted by Mn in the composition has already shown to generate a great increase in T_C (see $Tb_2Dy_4FeSb_2$ to $Tb_2Dy_4Fe_{0.75}Mn_{0.25}Sb_2$ in Fig. 2(a and c), and $Tb_6Ni_{0.75}Mn_{0.25}SbTe$ to $Tb_6Ni_{0.5}Mn_{0.5}SbTe$ in Fig. 2(b and d)), while a change in the p-block element has only shown to have a minor effect on the position of the Curie temperature.[29–31]

Three general trends regarding the effect of the *c* cell parameter on the Curie temperature have been detected in this study. On one hand, the three compounds with a larger *c* cell parameter, which are the ones with Dy_4 and Sb_2 in their composition (compounds 2, 3, and 4 as labelled in Table 1), show a linear increase of T_C following the *c* cell parameter (see Fig. 3s in the ESI†). On the other hand, a similar trend is observed for the compounds without Dy and with SbTe instead of Sb_2 (compounds 1, 5, 6 and 7 as labelled in Table 1). Finally, the compounds with a lower *c* cell parameter, which are the ones containing Ni (compounds 8 and 9 as labelled in Table 1), do not follow any of the previous trends, generating their own linear tendency as clearly shown in Fig. 3s.†

Additional peaks and inflections to the ones corresponding to T_C and T_m can be observed in Fig. 2(c and d) for some compounds. These peaks are not observed in the samples containing a single phase ($Tb_6Fe_{0.75}Mn_{0.25}SbTe$ and $Gd_3Tb_3FeSbTe$), and only in those with a small amount of secondary phase we do find additional peaks. Although this might lead to the conclusion that the secondary phase is responsible for the peaks, this does not seem to be the case. In both $Tb_2Dy_4FeSb_2$ and $Tb_2Dy_4Fe_{0.75}Mn_{0.25}Sb_2$ there is a small amount of $Tb_{1.7}Dy_{3.3}Sb_3$ (5 wt% and 4 wt% respectively), however, the additional peaks appear at very different temperatures for each compound. This suggests that these peaks can be attributed to additional spin reorientation mechanisms, given the complex magnetic structures of these compounds. The magnetism of $Tb_{1.7}Dy_{3.3}Sb_3$, $Gd_{1.8}Dy_{3.2}Sb_3$, $Gd_{0.34}Dy_{0.66}$, (in $Gd_2Dy_4Fe_{0.75}Mn_{0.25}Sb_2$, 6 wt% and <1 wt% respectively), $Gd_{0.33}Tb_{0.67}$ (in $Gd_2Tb_4Fe_{0.75}Mn_{0.25}SbTe$, 3 wt%), $Tb_{64.3}Sb_{21.3}Te_{14.4}$ and $Tb_{49.7}Sb_{21.1}Te_{29.2}$, the latter two observed in $Tb_6Ni_{0.5}Mn_{0.5}SbTe$ (4 wt% and 1 wt%, respectively), has not been reported in the literature. Finally, the small bump at around 227 K visible in Fig. 2(d) for $Tb_6Co_{0.75}Mn_{0.25}SbTe$ and $Tb_6Ni_{0.75}Mn_{0.25}SbTe$ can be attributed to the small amount of Tb in both samples. Full information regarding the alloy's content can be found in Table 1s in the ESI.†

Fig. 3 shows the hysteresis loops at 2 K (a and c) and 100 K (b and d) for all the compounds. In all the cases, at 2 K, we can observe the existence of a coercive field (H_C) and the metamagnetic field induced transitions exhibiting a step-like behavior. Except for Ni containing compounds (which show very similar loops), SbTe compounds show a single high step in the loops at 2 K, while the Sb_2 compounds have multiple smaller steps, indicating intermediate states with coexisting magnetic phases. These phenomena, which quickly disappear when the temperature is increased (as can be observed at 100 K), point to the antiferromagnetic components in the ground state of these compounds, which are responsible for the formation of complex non-collinear magnetic structures in this temperature region. Saturation magnetization values are very high in every case, with higher values being obtained for the Sb_2 compounds, from 155 emu g^{-1} for $Gd_2Tb_2FeSbTe$ to 228 emu g^{-1} for $Tb_2Dy_4FeSb_2$.

In order to confirm the order of the magnetic phase transitions, the Banerjee criterion has been applied, according to which, when representing M^2 as a function of H/M (Arrot plot), negative slopes would indicate a first order transition and positive ones a second order transition. All the compounds in this study show positive slopes in the Arrot plots, thus confirming the second order nature of the transitions. The Arrot plot for $Tb_6Fe_{0.75}Mn_{0.25}SbTe$ is presented in Fig. 4s† as an example.

3.3. Critical behavior

As explained in the Introduction section, important information about the physical systems can be retrieved from the study of the critical behavior of their second order magnetic phase transitions. Scaling analysis within the framework of renormalization group theory states that second order phase transitions can be characterized by some critical exponents related to physical properties such as spontaneous magnetization (M_S), the inverse of the initial susceptibility (χ_0^{-1}) or the critical isotherm. These parameters can be described according to the following scaling laws in the vicinity of T_C:[48]

$$M_S(T) \sim |t|^{\beta} \ (T < T_C) \quad (1)$$

$$\chi_0^{-1}(T) \sim |t|^{\gamma} \ (T > T_C) \quad (2)$$

$$M(H) \sim H^{1/\delta} \ (T = T_C) \quad (3)$$

where $t = (T - T_C)/T_C$ is the reduced temperature and β, γ, and δ are the critical exponents associated with the different magnetic properties. As will be shown later, these critical exponents will also allow the extrapolation of magnetocaloric properties to magnetic field values that may not be experimentally reachable. The precise value of the critical exponents is ensured by a well-established iteration method and by checking the obtained results with the scaling relations they must obey. In order to have higher precision, magnetization isotherms in the neighbourhood of the corresponding T_C are measured every 1 K.

The first step consists of representing for each sample the Modified Arrot Plots (MAP), where $M^{1/\beta}$ is presented *versus* $(H/M)^{1/\gamma}$. The initial critical exponent values are selected to match those of the most common universality classes for magnetic materials (mean field: β = 0.5, γ = 1.0; 3D-Heisenberg: β = 0.369, γ = 1.396; 3D-Ising: β = 0.3265 and γ = 1.237[48–50] (see Table 2s†)). Straight parallel lines in the MAP would indicate that the critical exponents used are the correct ones. In every

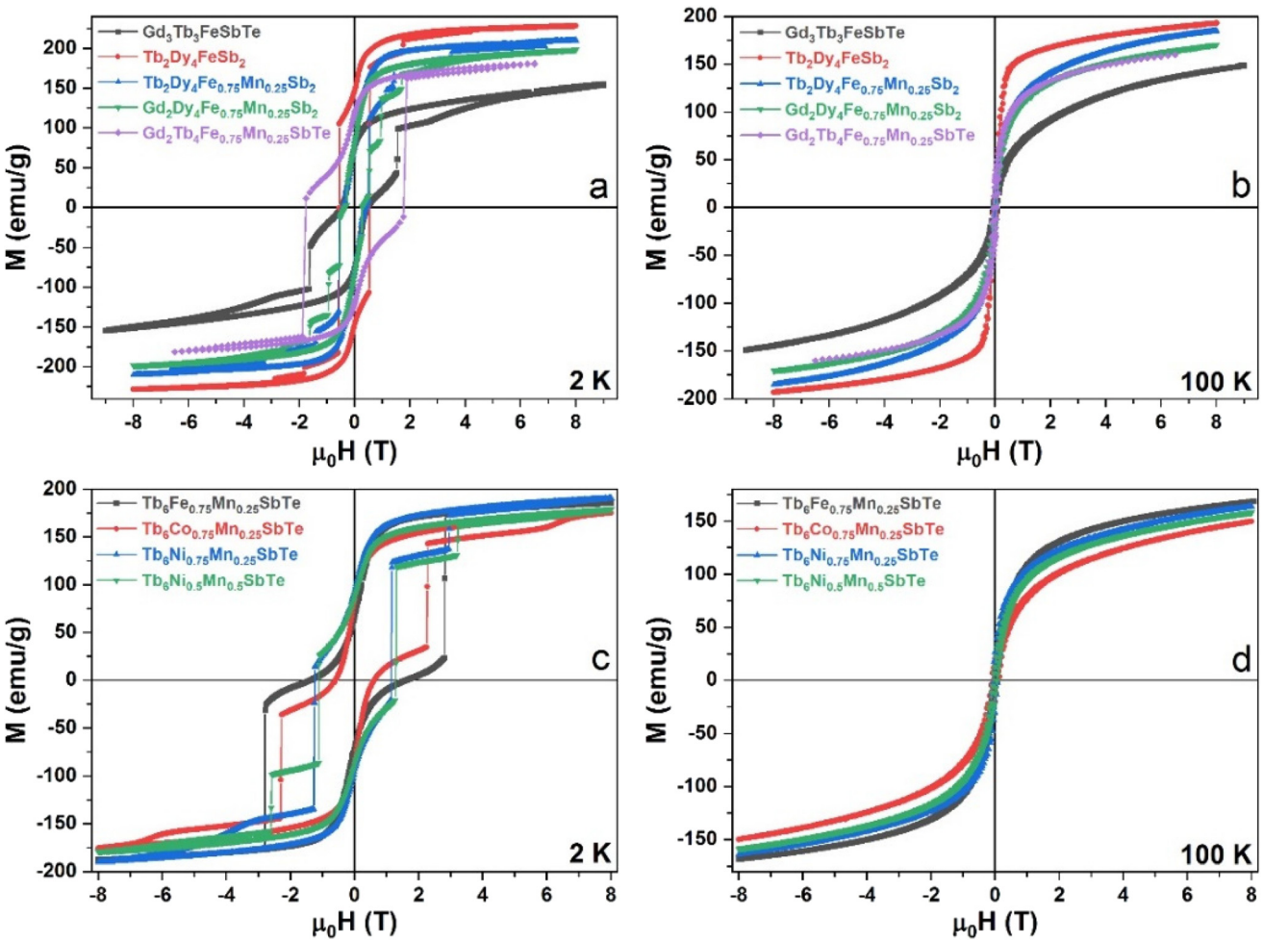

Fig. 3 Isothermal magnetic hysteresis loops at 2 K (a) and (c) and at 100 K (b) and (d) for $Gd_3Tb_3FeSbTe$, $Tb_2Dy_4FeSb_2$, $Tb_2Dy_4Fe_{0.75}Mn_{0.25}Sb_2$, $Gd_2Dy_4Fe_{0.75}Mn_{0.25}Sb_2$, and $Gd_2Tb_4Fe_{0.75}Mn_{0.25}Sb_2$ (a) and (b), and for $Tb_6Fe_{0.75}Mn_{0.25}SbTe$, $Tb_6Co_{0.75}Mn_{0.25}SbTe$, $Tb_6Ni_{0.75}Mn_{0.25}SbTe$ and $Tb_6Ni_{0.5}Mn_{0.5}SbTe$ (c) and (d).

case the Mean Field (MF) model yields the best results, but only for $Tb_2Dy_4FeSb_2$ there was an optimal starting point for the iterative procedure. As we already observed for previously studied compounds belonging to the R_6TX_2 family,[29–31] the critical behavior of the remaining compounds cannot be described by any known universality class, which means that we had to map β and γ values searching for good initial values, *i.e.*, where we get straight parallel lines in the MAP. The values thus obtained are then adjusted in an iterative procedure, for which we extract M_S and χ_0^{-1} by linear extrapolation from the high field data in the MAP. These values are then fitted to eqn (1) and (2) to obtain new β and γ values. Then the MAP is again represented with the new critical exponent values and its linearity and parallelism are inspected. The process is repeated until the best values of β and γ are obtained. In the case of $Tb_2Dy_4FeSb_2$, any deviation of the critical exponents from those corresponding to the MF model worsened the parallelism and straightness of the isotherms in the MAP, while for the other materials different starting points had to be tested to find the best results.

When the MAP is represented by using the correct critical exponent values, the critical isotherm should intersect the (0, 0) point. This critical isotherm can be fitted to eqn (3) in order to get the third magnetic critical exponent, δ. The value of δ obtained by this method can be compared to the one obtained using the Widom scaling equation:[43]

$$\delta = 1 + \gamma/\beta \tag{4}$$

where β and γ are the previously obtained parameters for each compound.

Finally, the most robust confirmation of the obtained critical exponents is given by the fulfillment of the magnetic equation of state, as follows:

$$M(H,t) = |t|^{\beta} f_{\pm}(H/|t|^{\beta+\gamma}) \tag{5}$$

Here t is the reduced temperature. This expression states that for the correct β and γ values the magnetic isotherms must collapse into two independent branches, one for isotherms below the critical temperature and another one above

it (indicated by – and + sub-indexes, respectively). The final MAPs, the fitting of the critical isotherms and the fulfillment of the magnetic equation of state of every compound are shown in Fig. 4, confirming that the critical exponent values obtained are the correct ones. These values are collected in Table 2.

Fig. 4 shows from left to right the MAP, critical isotherm and the fulfillment of the magnetic equation of state for 3 of the 9 compounds: $Tb_2Dy_4FeSb_2$, $Gd_2Tb_4Fe_{0.75}Mn_{0.25}SbTe$ and $Tb_6Fe_{0.75}Mn_{0.25}SbTe$. The rest of the compounds are very similar and can be observed in Fig. 5s and 6s in the ESI.† The fittings are very good in all cases.

Regarding the obtained critical exponent values, we can see from Table 2 that in every case the δ values retrieved from the critical isotherms match those calculated using eqn (4), validating our results. The value of γ is directly related to the range of the exchange interaction $J(r)$.[51] With the exception of $Gd_2Tb_4Fe_{0.75}Mn_{0.25}SbTe$ and $Tb_6Co_{0.75}Mn_{0.25}SbTe$, γ has a value very close or equal to 1, and this points to a long range magnetic interaction described by the MF universality class. In the case of $Gd_2Tb_4Fe_{0.75}Mn_{0.25}SbTe$, $\gamma_{exp} = 1.30 \pm 0.03$ is closer to the 3D-XY model ($\gamma_{xy} = 1.317$), while for $Tb_6Co_{0.75}Mn_{0.25}SbTe$ $\gamma_{exp} = 0.86 \pm 0.04$ is lower than the expected value for any known theoretical model. Furthermore,

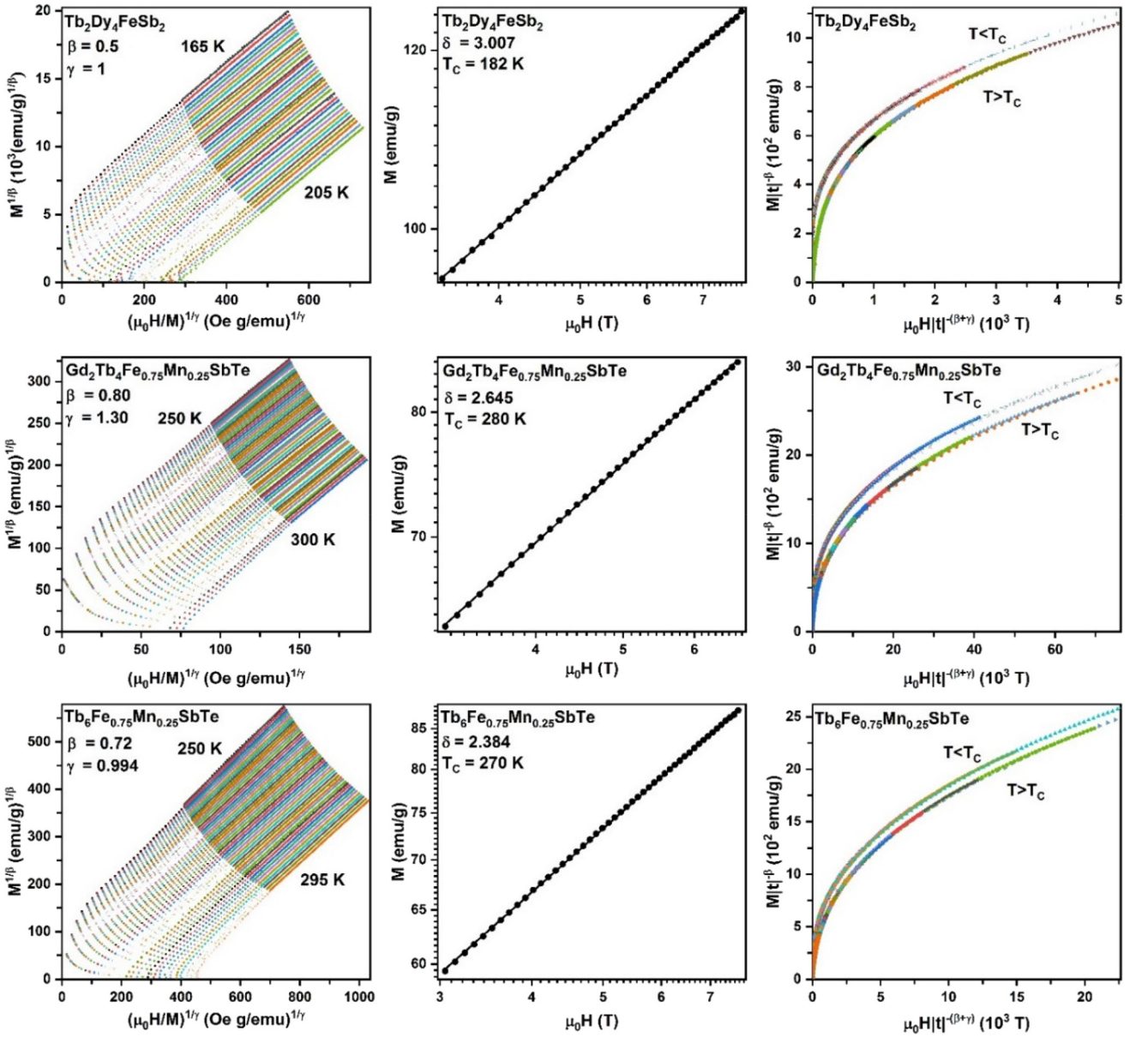

Fig. 4 From left to right: optimized modified Arrot plot, *M vs.* $\mu_0 H$ plot on the logarithmic scale for the critical isotherm and representation of the magnetic equation of state for $Tb_2Dy_4FeSb_2$ (the top row), $Gd_2Tb_4Fe_{0.75}Mn_{0.25}SbTe$ (the middle row) and $Tb_6Fe_{0.75}Mn_{0.25}SbTe$ (the bottom row).

Table 2 The magnetic critical exponents obtained for the nine studied compounds

N	Material	β	γ	δ^a	δ (critical isotherm)
1	$Gd_3Tb_3FeSbTe$	0.59 ± 0.02	0.98 ± 0.03	2.66 ± 0.09	2.649 ± 0.009
2	$Tb_2Dy_4FeSb_2$	0.50 ± 0.01	1.0 ± 0.02	3.00 ± 0.04	3.007 ± 0.005
3	$Tb_2Dy_4Fe_{0.75}Mn_{0.25}Sb_2$	0.90 ± 0.03	0.98 ± 0.04	2.09 ± 0.08	2.093 ± 0.005
4	$Gd_2Dy_4Fe_{0.75}Mn_{0.25}Sb_2$	0.80 ± 0.01	1.03 ± 0.02	2.29 ± 0.04	2.321 ± 0.003
5	$Gd_2Tb_4Fe_{0.75}Mn_{0.25}SbTe$	0.80 ± 0.01	1.30 ± 0.03	2.63 ± 0.06	2.645 ± 0.006
6	$Tb_6Fe_{0.75}Mn_{0.25}SbTe$	0.72 ± 0.01	0.994 ± 0.007	2.38 ± 0.03	2.384 ± 0.004
7	$Tb_6Co_{0.75}Mn_{0.25}SbTe$	0.78 ± 0.02	0.86 ± 0.04	2.10 ± 0.07	2.093 ± 0.006
8	$Tb_6Ni_{0.75}Mn_{0.25}SbTe$	0.70 ± 0.01	1.02 ± 0.04	2.44 ± 0.09	2.451 ± 0.005
9	$Tb_6Ni_{0.5}Mn_{0.5}SbTe$	0.615 ± 0.009	0.93 ± 0.01	2.51 ± 0.03	2. 513 ± 0.004

[a] δ is calculated from eqn (4) using β and γ values obtained by the iterative MAP method and δ (critical isotherm) is the value directly obtained by the fitting of the critical isotherm.

except for $Tb_2Dy_4FeSb_2$, the β values do not agree with the MF model; in fact they are higher (0.59–0.90) than the ones found for any other known universality classes (see Table 2s in the ESI†).[48–50,52–57] These high β values are in agreement with our previous studies; in fact, for $Tb_6Fe_{0.75}Mn_{0.25}SbTe$ (β_{exp} = 0.72 ± 0.01) β is very close to those of other Tb_6(Fe, Mn)X_2 compounds, such as $Tb_6Fe_{0.5}Mn_{0.5}Bi_2$ (β_{exp} = 0.72 ± 0.02) or Tb_6FeBi_2 (β_{exp} = 0.73 ± 0.09).[30] In the same way, $Gd_3Tb_3FeSbTe$ shows a similar β value (β_{exp} = 0.59 ± 0.02) to that of $Gd_3Tb_3FeBi_2$ (β_{exp} = 0.58 ± 0.02), as also shown in ref. 30. The most striking result comes from the difference between $Tb_2Dy_4FeSb_2$ and $Tb_2Dy_4Fe_{0.75}Mn_{0.25}Sb_2$, where a 25% increase of Mn moves β from 0.5 to 0.9 ± 0.03. To account for these results a deeper knowledge of the complex hybridization process combined with theoretical work addressing large β values is needed, since the already developed universality classes do not match these values.

3.4. Magnetocaloric properties

The magnetocaloric properties of all of the compounds have been evaluated in terms of magnetic entropy change (ΔS_M), refrigerant capacity (RC) and temperature averaged entropy change (TEC). The magnetic entropy change has been indirectly obtained from magnetization measurements using the well-known Maxwell relation.[1] The results of all the compounds are shown in Fig. 5 and 6 for $\mu_0\Delta H$ from 0.5 to 7.9 T (except for $Gd_2Tb_4Fe_{0.75}Mn_{0.25}SbTe$, which was only measured up to 7 T). Two peaks corresponding to T_C and T_m can be observed, creating the expected plateau region in between, which increases the refrigerant capacity value and the efficiency of an Ericsson thermodynamic refrigeration cycle.[1]

It should be noticed that no additional contribution of small secondary phases to $Tb_2Dy_4FeSb_2$, $Tb_2Dy_4Fe_{0.75}Mn_{0.25}Sb_2$ and $Gd_2Dy_4Fe_{0.75}Mn_{0.25}Sb_2$ can be observed in Fig. 5. This confirms that the only relevant contribution to the magnetocaloric effect comes from the main phase. Fig. 6 shows that the ΔS_M shape of the Tb_6(Fe, Co, Ni)$_X$Mn$_{1-X}$SbTe family is very similar.

Usually, ΔS_M data are accompanied by the refrigerant capacity (RC), which is considered a key parameter to characterize the performance of a magnetocaloric material as a magnetic refrigerator. The refrigerant capacity is typically represented by RC_{FWHM} (obtained by multiplying the width at half the value of the peak times the value of the peak) or RC_{Area} (the area enclosed by the peak between the points where ΔS_M is half the value of the peak). However, when the peak of the magnetocaloric effect is very wide (shallow peaks) or when it gets wider due to the presence of other transitions (which is our case), the RC values are artificially enlarged. In order to avoid an overestimation of the potential of these materials, some studies propose the use of the temperature averaged entropy change TEC (10),[17,58] which is defined as:

$$\mathrm{TEC}(10) = \frac{1}{10}\int_{T^{pk}-5}^{T^{pk}+5} \Delta S_M(T')\mathrm{d}T' \quad (6)$$

where T^{pk} is the temperature at the peak of the magnetic entropy change. The magnetic entropy change, RC and TEC (10), values at T_C and T_m for $\mu_0\Delta H$ equal to 2 T and 5 T are collected in Table 3. These fields have been chosen in order to allow the comparison of our results with that in the literature.

The highest peak of the magnetic entropy change is found for $Tb_2Dy_4FeSb_2$ around 182 K ($|\Delta S_M(T_C, 5\ T)|$ = 7.72 J kg^{-1} K^{-1}), which is the material with the lowest T_C. Although the substitution of 25% of Fe by Mn in order to obtain $Tb_2Dy_4Fe_{0.75}Mn_{0.25}Sb_2$ results in an increase of the Curie temperature, it also causes a decrease of the magnetic entropy peak to less than half of the one observed in the previous compound. However, the value of the peak at T_m is only slightly reduced. For the other compounds $|\Delta S_M\ (T_C, 5\ T)|$ values at T_C lie in the range of 2.88–4.53 J kg^{-1} K^{-1}, where the lowest value is found for $Gd_2Dy_4Fe_{0.75}Mn_{0.25}Sb_2$ and the highest one for $Tb_6Ni_{0.75}Mn_{0.25}SbTe$. The latter shows the highest magnetic entropy change value among the Tb_6(Fe,Co,Ni)$_{0.75}$Mn$_{0.25}$SbTe samples. Furthermore, as for $Tb_2Dy_4FeSb_2$, the peak value of $Tb_6Ni_{0.75}Mn_{0.25}SbTe$ decreases as the amount of Mn does, and therefore T_C increases. Regarding the RC_{FWHM} values, –Sb_2 compounds clearly show higher values at 5 T than the ones obtained for –SbTe compounds, with the latter having sharper peaks.

The results obtained in this work have been compared with the ones obtained for previous R_6TX_2 intermetallic family compounds. Fig. 7 shows a comparison of T_C (where PM–FM transition takes place), $-\Delta S_M$ (T_C, 5 T) and RC_{FWHM} values for Ho_6(Fe,Mn)Bi_2,[29] (Gd,Tb)$_6$(Fe,Mn)Bi_2,[30] and Dy_6(Fe,Mn)X_2 [31] compounds and the ones studied in this work. The improve-

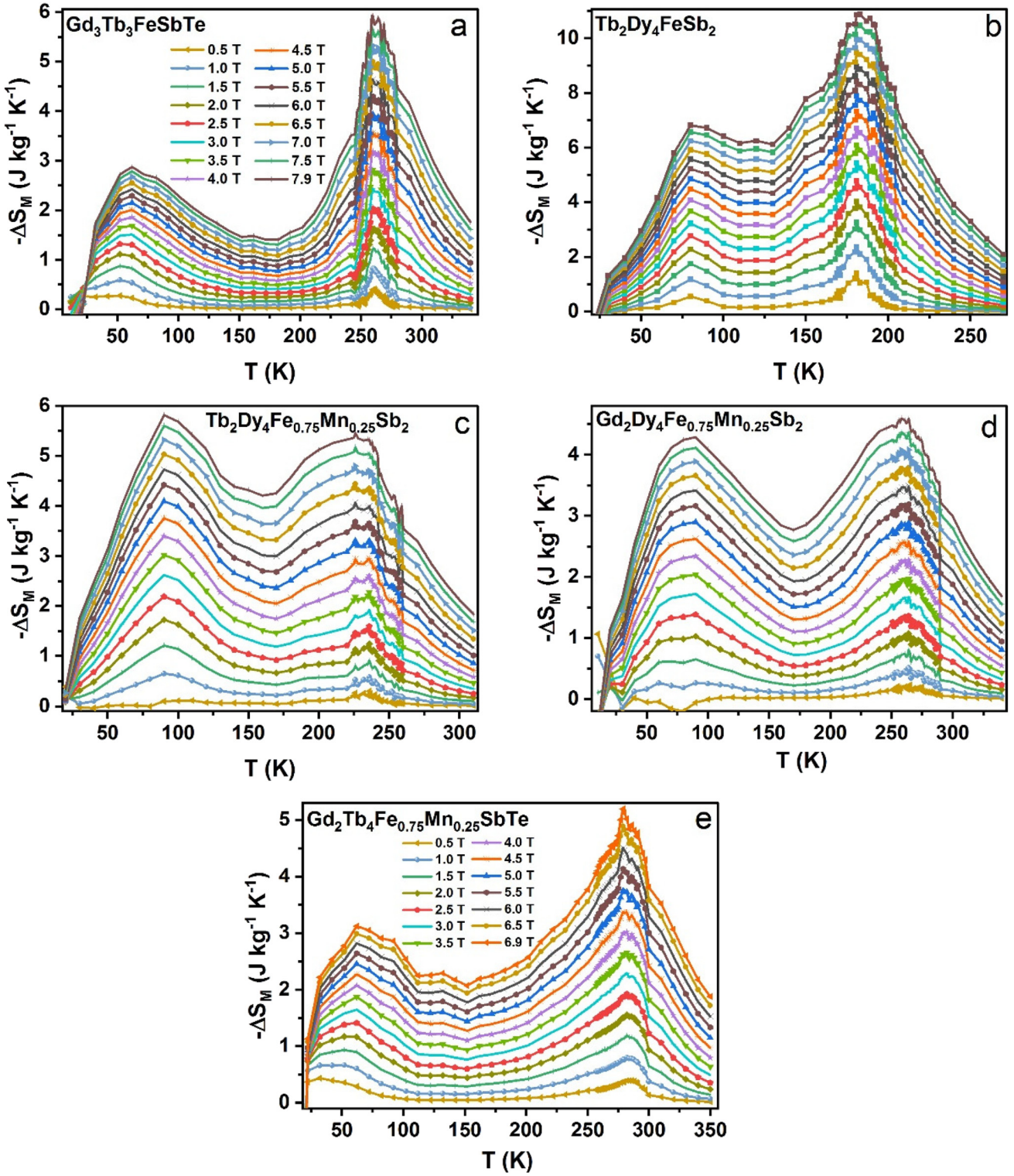

Fig. 5 Magnetic entropy change $-\Delta S_M$ for $Gd_3Tb_3FeSbTe$ (a), $Tb_2Dy_4FeSb_2$ (b), $Tb_2Dy_4Fe_{0.75}Mn_{0.25}Sb_2$ (c), $Gd_2Dy_4Fe_{0.75}Mn_{0.25}Sb_2$ (d) and $Gd_2Tb_4Fe_{0.75}Mn_{0.25}SbTe$ (e). The colour code is the same for all of them.

ment with respect to previous compounds can be clearly seen. First of all, the Curie temperatures of 8 out of 9 new compounds are located closer to room temperature than previous ones, with the exception of Tb_6FeBi_2 [30] and $Dy_6Fe_{0.5}Mn_{0.5}Bi_2$,[31] which were already close to room temperature. However, the newly studied compounds show either better working temperatures (compounds 1, 4, 5, 6, 8 and 9) than Tb_6FeBi_2 and $Dy_6Fe_{0.5}Mn_{0.5}Bi_2$ or higher RC_{FWHM} values than Tb_6FeBi_2

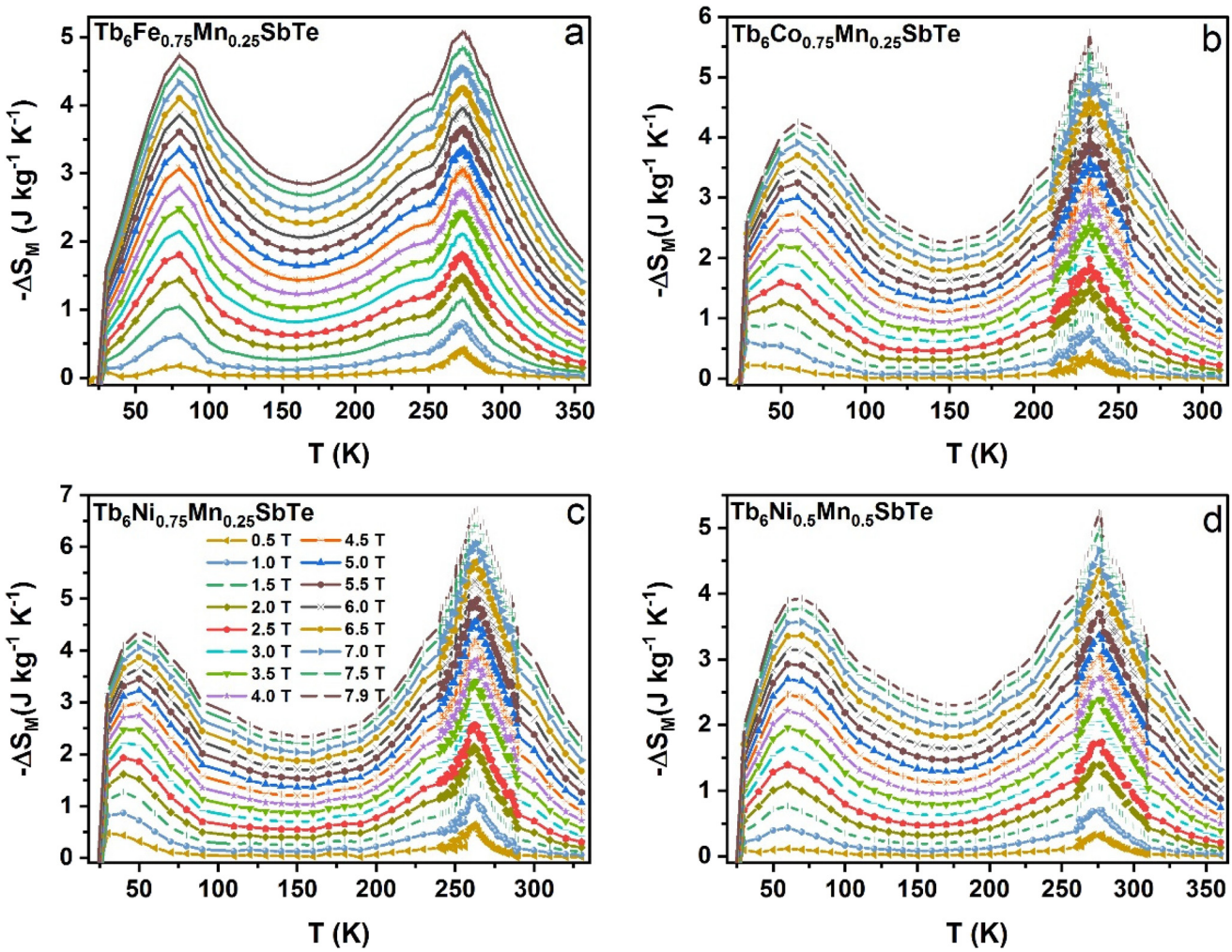

Fig. 6 Magnetic entropy change $-\Delta S_M$ for $Tb_6Fe_{0.75}Mn_{0.25}SbTe$ (a), $Tb_6Co_{0.75}Mn_{0.25}SbTe$ (b), $Tb_6Ni_{0.75}Mn_{0.25}SbTe$ (c) and $Tb_6Ni_{0.5}Mn_{0.5}SbTe$ (d). The colour code is the same for all of them.

Table 3 Absolute value of the magnetic entropy change $|\Delta S_M|$, refrigerant capacities RC_{FWHM} and RC_{Area}, and temperature averaged entropy change TEC (10) at different applied fields ($\mu_0\Delta H$ = 2 and 5 T). Values are given for both peaks of the 9 compounds, at T_m and T_C

		2 T				5 T			
		$\lvert\Delta S_M\rvert$ (J kg^{-1} K^{-1})	RC_{FWHM} (J kg^{-1})	RC_{Area} (J kg^{-1})	TEC (10) (J kg^{-1} K^{-1})	$\lvert\Delta S_M\rvert$ (J kg^{-1} K^{-1})	RC_{FWHM} (J kg^{-1})	RC_{Area} (J kg^{-1})	TEC (10) (J kg^{-1} K^{-1})
(1) $Gd_3Tb_3FeSbTe$	T_C (260 K)	1.62	45.67	34.96	1.43	3.93	212.61	157.44	3.73
	T_m (62 K)	1.11	78.58	62.25	1.09	2.15	215.13	167.02	2.11
(2) $Tb_2Dy_4FeSb_2$	T_C (182 K)	3.81	202.89	146.01	3.55	7.72	1103.04	729.52	7.45
	T_m (85 K)	2.25	333.49	305.23	2.09	4.79	842.67	829.25	4.68
(3) $Tb_2Dy_4Fe_{0.75}Mn_{0.25}Sb_2$	T_C (233 K)	1.24	259.48	213.68	1.14	3.30	768.33	668.49	3.19
	T_m (90 K)	1.72	141.86	108.47	1.67	4.09	864.04	629.24	4.00
(4) $Gd_2Dy_4Fe_{0.75}Mn_{0.25}Sb_2$	T_C (264 K)	1.07	82.73	61.27	1.01	2.88	778.38	520.93	2.82
	T_m (90 K)	1.02	104.54	82.96	1.00	2.90	780.78	590.21	2.86
(5) $Gd_2Tb_4Fe_{0.75}Mn_{0.25}SbTe$	T_C (282 K)	1.56	138.79	101.75	1.51	3.72	451.25	327.89	3.65
	T_m (62 K)	1.16	93.65	76.89	1.14	2.46	787.95	685.10	2.40
(6) $Tb_6Fe_{0.75}Mn_{0.25}SbTe$	T_C (273 K)	1.49	114.94	79.23	1.40	3.35	470.03	329.97	3.27
	T_m (80 K)	1.44	87.95	68.40	1.39	3.35	368.48	267.93	3.28
(7) $Tb_6Co_{0.75}Mn_{0.25}SbTe$	T_C (234 K)	1.46	65.58	49.67	1.35	3.55	275.92	199.43	3.38
	T_m (60 K)	1.27	72.63	59.90	1.23	2.99	255.61	202.53	2.94
(8) $Tb_6Ni_{0.75}Mn_{0.25}SbTe$	T_C (262 K)	2.08	104.40	72.96	1.84	4.53	334.20	242.11	4.25
	T_m (50 K)	1.60	72.11	59.17	1.56	3.21	264.09	201.07	3.16
(9) $Tb_6Ni_{0.5}Mn_{0.5}SbTe$	T_C (272 K)	1.40	87.20	62.54	1.30	3.33	323.43	230.73	3.15
	T_m (60 K)	1.08	77.22	61.03	1.05	2.69	318.20	238.65	2.66

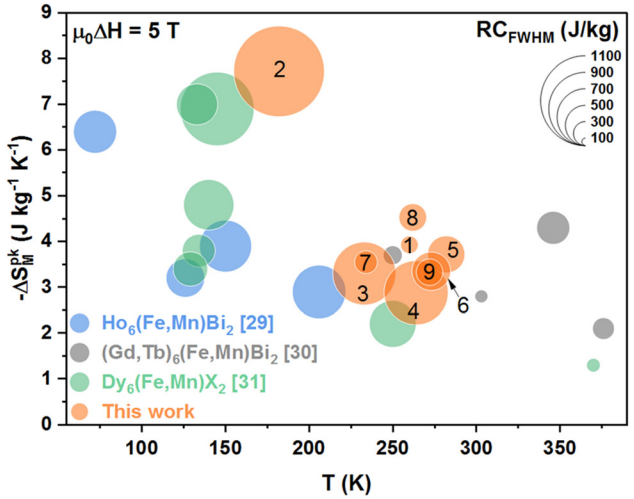

Fig. 7 Comparison of T_C, $-\Delta S_M$ (T_C, 5 T) and RC_{FWHM} values for $Ho_6(Fe,Mn)Bi_2$ (blue),[29] $(Gd,Tb)_6(Fe,Mn)Bi_2$ (grey),[30] $Dy_6(Fe,Mn)X_2$ (green)[31] compounds and the ones studied in this work (orange). Number labels are the ones used in Tables 1–4 and Table 1s.†

(compounds 3, 4, 5, 6, 8 and 9) or $Dy_6Fe_{0.5}Mn_{0.5}Bi_2$ (compounds 3 and 4). Furthermore, $|\Delta S_M\ (T_C, 5\ T)|$ is in every case higher than the ones obtained for $Dy_6Fe_{0.5}Mn_{0.5}Bi_2$. Finally, $Tb_2Dy_4FeSb_2$ shows a lower T_C; however, it is still higher than the ones for most of the previously studied compounds, and exhibits the greatest performance in its temperature range. Overall, the goal of improving the magnetocaloric performances has been achieved.

The magnetic entropy change values at T_C for $\mu_0\Delta H = 5$ T can also be compared to the ones collected in Fig. 25 of the extensive review on magnetocaloric materials by V. Franco *et al.*[1] The aforementioned figure shows ΔS_M values for rare-earth containing compounds in the range of 0 to 350 K. It can be immediately observed that the $|\Delta S_M|$ of $Tb_2Dy_4FeSb_2$ lies among the highest ones in its temperature range, and the remaining ones have average values compared to the other room temperature compounds.

It has been proven that, in the particular case of second order magnetic phase transitions, a universal curve for the magnetic entropy change can be built up. The existence of such a master curve is used to check the nature of the transition.[59] This universal curve involves the collapse of the magnetic entropy change curves at different fields into a single one. The process consists of first normalizing each $\Delta S_M(H,T)$ curve with respect to the corresponding maximum value and, then, rescaling the temperature axis by using a reference temperature, T_r. This T_r is selected to be above T_C and it corresponds to a particular fraction of $\Delta S_M(T_C)$, which in this case is 0.5. The temperature axis rescaling is then performed as follows:

$$\theta = \frac{T - T_C}{T_r - T_C} \tag{7}$$

The results of the universal curve thus obtained for $Gd_3Tb_3FeSbTe$ are shown in the left part of Fig. 8 as an example. The fact that these master curves can be obtained ensures that the magnetic phase transition at T_C has a second order nature, as has been previously shown. Nevertheless, the utility of universal curves is beyond this confirmation. When universal curves are combined with magnetocaloric scaling laws, ΔS_M curves at any field can be obtained by reversing the process, even for magnetic fields or temperatures which cannot be experimentally measured. For instance, the peak maximum of the magnetic entropy change is given as:

$$\Delta S_M^{pk} \sim H^{1+\frac{1}{\delta}\left(1-\frac{1}{\beta}\right)} \tag{8}$$

where δ and β are the magnetic critical exponents that we have already obtained for each compound (see Table 2). When the

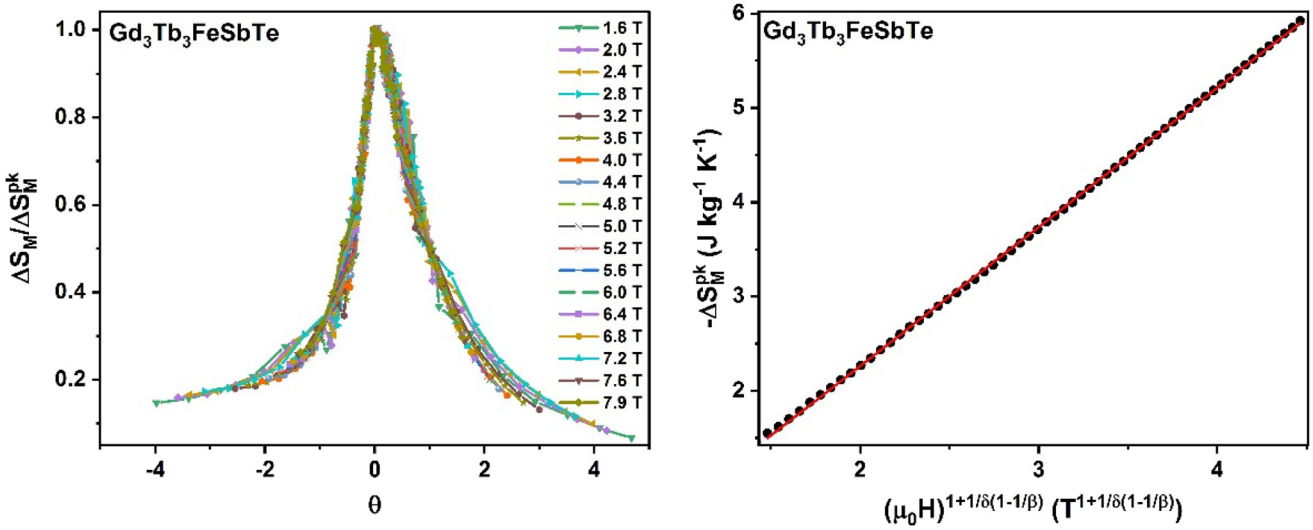

Fig. 8 Universal master curve (left) and scaling of the magnetic entropy change peak (right) for $Gd_3Tb_3FeSbTe$. β and γ values are the ones presented in Table 2.

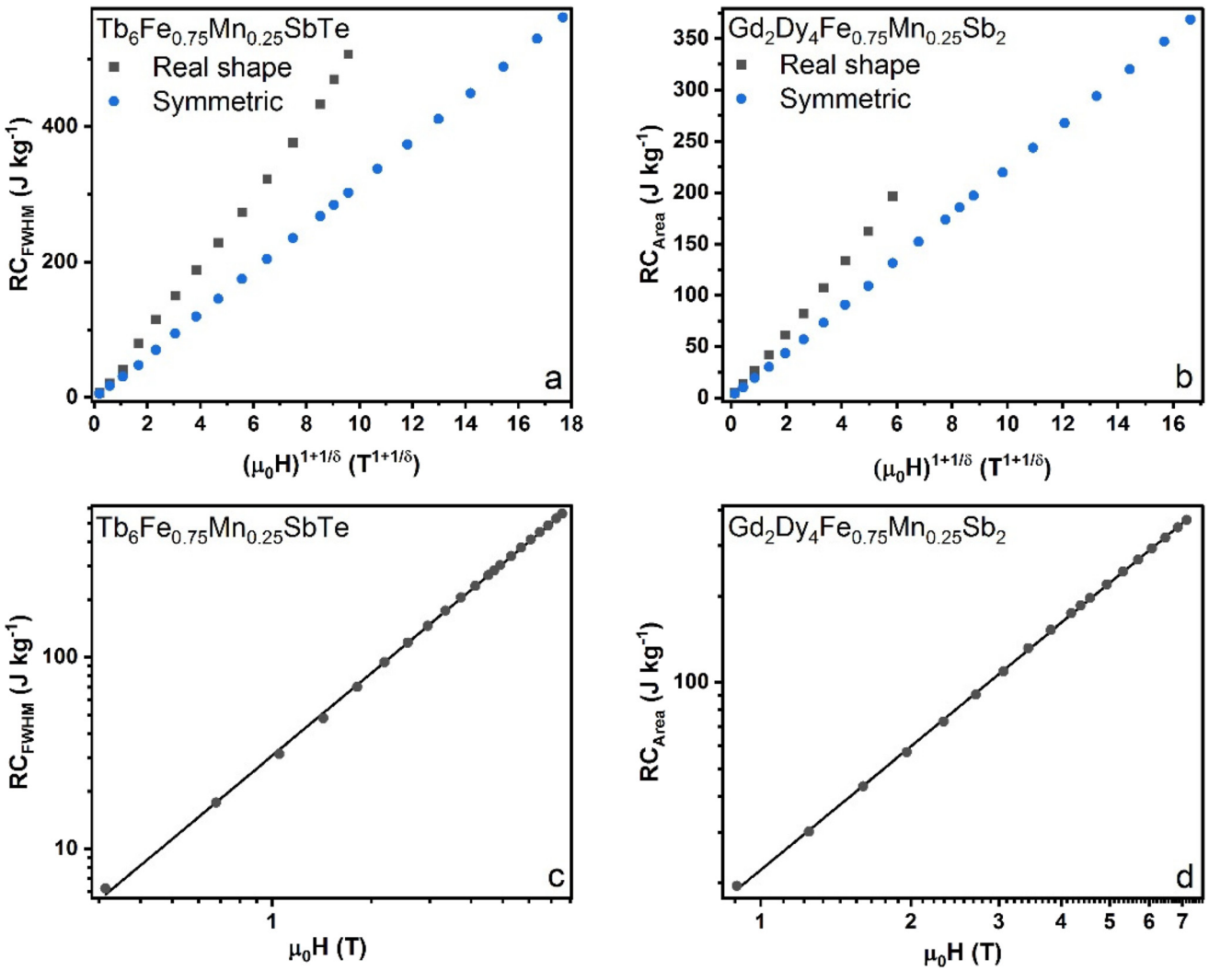

Fig. 9 Upper boxes: field dependence of RC_{FWHM} for $Tb_6Fe_{0.75}Mn_{0.25}SbTe$ (a) and RC_{Area} for $Gd_2Dy_4Fe_{0.75}Mn_{0.25}Sb_2$ (b). Black squares represent the values obtained using the real shape of the peak and blue circles represent the values obtained when the peak is considered symmetric. The δ values are the ones presented in Table 2. Lower boxes: RC_{FWHM} (c) and RC_{Area} (d) *vs.* $\mu_0 H$ log–log scale representation and fitting, for $Tb_6Fe_{0.75}Mn_{0.25}SbTe$ (c) and $Gd_2Dy_4Fe_{0.75}Mn_{0.25}Sb_2$ (d).

experimental data are presented following eqn (8), all the points must fall along a straight line if the correct critical exponents are used. This is in fact what can be observed for $Gd_3Tb_3FeSbTe$ in the right hand part of Fig. 8, confirming, once again, that the correct values of the critical exponents have been obtained and allowing the extrapolation of the data to desirable magnetic fields. The red line in the graph shows a linear fit in order to serve as a visual guide.

Moreover, for second order magnetic phase transitions both refrigerant capacities previously described (RC_{FWHM} and RC_{Area}) must obey the following scaling relation:

$$RC \propto H^{1+1/\delta} \quad (9)$$

where δ is the critical exponent related to the critical isotherm (eqn (3)). However, this scaling relation does not hold when the width of the peak is enlarged by the effect of another magnetic phase transition generating a second peak. In fact, in some of these materials, as the field is increased and the peak at the Curie temperature gets wider, and the point at $T_r < T_C$ for which $\Delta S_M(T_r) = \Delta S_M(T_C)/2$ is below T_m. This is responsible for the high RC values obtained for several compounds (see Table 3). Instead, we will show that a symmetric peak approach can be taken to satisfy eqn (9). $Tb_6Fe_{0.75}Mn_{0.25}SbTe$ and $Gd_2Dy_4Fe_{0.75}Mn_{0.25}Sb_2$ will be used as an example, but the same results are obtained for the other compounds. The symmetric approach involves considering the higher temperature peak as if it was symmetric, *i.e.*, as if the lower temperature peak did not enlarge its width. This is done by obtaining the width of the peak as two times the distance (in the temperature axis) from T_C to the point above T_C where the magnetic entropy change takes half the value of the peak. The value of RC_{Area} is obtained as twice the area in the previous region.

Graphs (a) and (b) in Fig. 9 show the scaling of RC_{FWHM} for $Tb_6Fe_{0.75}Mn_{0.25}SbTe$ and of RC_{Area} for $Gd_2Dy_4Fe_{0.75}Mn_{0.25}Sb_2$, respectively. The critical exponent, δ, used in each case is the one obtained from their corresponding critical isotherm (see Table 2). In both cases, the RC values obtained from the usual definitions (considering the real shape of the peak) are represented in dark grey, while the values obtained when considering a symmetric peak are represented in blue. The data for the usual RCs are cut just before the field at which $\Delta S_M(T_r) = \Delta S_M(T_C)/2$ for $T_r < T_C$ is below T_m (4 T for $Tb_6Fe_{0.75}Mn_{0.25}SbTe$ and 5.2 T for $Gd_2Dy_4Fe_{0.75}Mn_{0.25}Sb_2$). From (a) and (b) graphs in Fig. 9 it can be clearly seen that the scaling only holds for the symmetric peak, for which all the points perfectly lie in a straight line, as they should. The convenience of using the symmetric peak has also been verified by fitting the experimental data to eqn (9) on a logarithmic scale in order to obtain the $\Delta' = 1 + 1/\delta$ parameter. The fittings can be observed in the (c) and (d) graphs of Fig. 9, and the values obtained have been compared to the Δ' values obtained for the δ exponents from the critical isotherms. For $Tb_6Fe_{0.75}Mn_{0.25}SbTe$ the fitted value is $\Delta'_{fit} = 1.437 \pm 0.007$, while the one obtained from δ is $\Delta'_{\delta} = 1.4195 \pm 0.0007$. In the case of $Gd_2Dy_4Fe_{0.75}Mn_{0.25}Sb_2$ $\Delta'_{fit} = 1.433 \pm 0.005$ and $\Delta'_{\delta} = 1.4308 \pm 0.0006$. The good agreement of these values confirms both the importance of considering the symmetry of the peak for good RC scaling, and the previously obtained critical exponent values.

3.5. Thermal properties

As important as the magnetic and magnetocaloric properties of magnetic refrigerants is their ability to exchange heat with their environment. This aspect has not been addressed in the literature as it corresponds. A material which is able to exchange heat quickly is required in order to work at high frequencies.[2,60] Among the thermal properties, thermal diffusivity (D) is the one describing the heat transfer under non-steady conditions. In these cases the spatial and time dependence of temperature, $T(r,t)$, is governed by the thermal diffusion equation.[61]

Table 4 Values of thermal properties, namely thermal diffusivity (D), thermal effusivity (e), specific heat capacity (c_p) and thermal conductivity (K), at 295 K

N	Material	D ($mm^2\ s^{-1}$)	e ($J\ m^{-2}\ K^{-1}\ s^{-1/2}$)	c_p ($J\ kg^{-1}\ K^{-1}$)	K ($W\ K^{-1}\ m^{-1}$)
1	$Gd_3Tb_3FeSbTe$	2.29	2626	203	3.97
2	$Tb_2Dy_4FeSb_2$	2.03	—	—	—
3	$Tb_2Dy_4Fe_{0.75}Mn_{0.25}Sb_2$	1.49	2457	231	3.00
4	$Gd_2Dy_4Fe_{0.75}Mn_{0.25}Sb_2$	1.86	2671	226	3.65
5	$Gd_2Tb_4Fe_{0.75}Mn_{0.25}SbTe$	1.84	2626	226	3.56
6	$Tb_6Fe_{0.75}Mn_{0.25}SbTe$	2.26	2612	201	3.92
7	$Tb_6Co_{0.75}Mn_{0.25}SbTe$	2.05	2336	187	3.34
8	$Tb_6Ni_{0.75}Mn_{0.25}SbTe$	2.14	2644	207	3.87
9	$Tb_6Ni_{0.5}Mn_{0.5}SbTe$	1.92	2402	200	3.33

The four thermal parameters which characterize any material (thermal diffusivity, D, thermal conductivity, K, thermal effusivity, e, and specific heat capacity, c_p) are related and only two of them are independent.[62] The ac photopyroelectric technique (PPE) in its back detection configuration allows the obtainment of a very high-resolution temperature dependence of thermal diffusivity.[36,63] This technique was used to extract D for all of our compounds around their paramagnetic to ferromagnetic phase transition, *i.e.*, around their expected working temperature. The result for $Tb_2Dy_4FeSb_2$ and $Tb_6Fe_{0.75}Mn_{0.25}SbTe$ can be observed in Fig. 10. The results for the remaining ones are collected in Fig. 7s and 8s, in the ESI.† All the compounds studied here exhibit thermal diffusivity values in the range of 1.3–2.3 $mm^2\ s^{-1}$. Although few D data in magnetocaloric materials are available in the literature, the values found in this study are comparable to the ones exhibited by $Gd_5Si_2Ge_2$ and $La(Fe_{0.88}Si_{0.12})_{13}$, which are two well-known good magnetocaloric materials, or even an order of magnitude higher than the ones found for MnAs.[60] The obtained values are similar to those previously observed in the $Dy_6(Fe,Mn)X_2$ (X = Sb, Bi, Te) intermetallic family.[31]

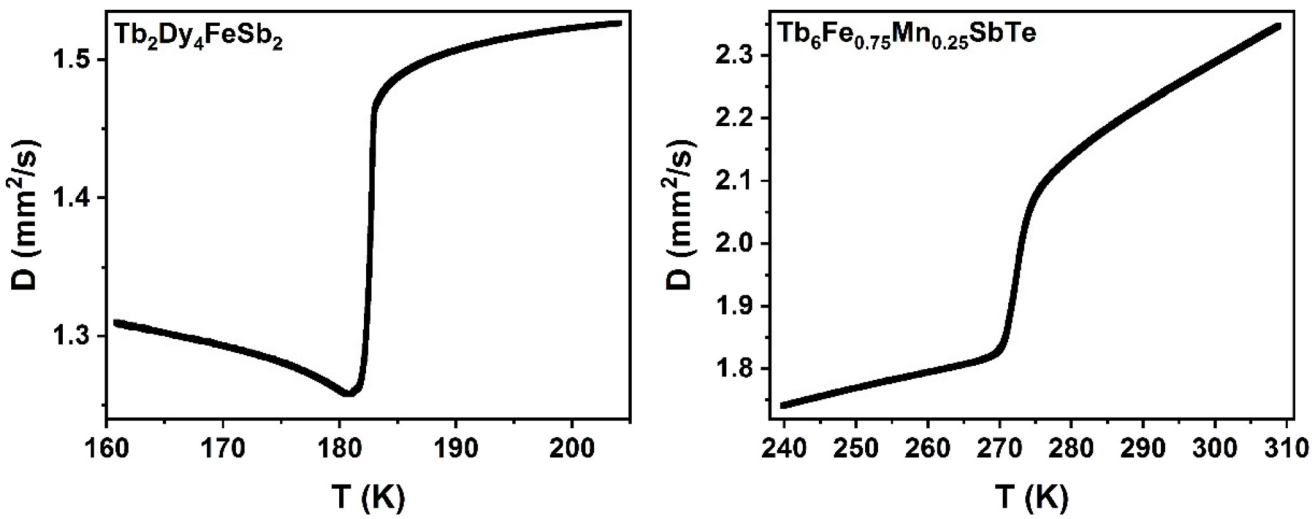

Fig. 10 Thermal diffusivity as a function of temperature around T_C for $Tb_2Dy_4FeSb_2$ (left) and $Tb_6Fe_{0.75}Mn_{0.25}SbTe$ (right).

Finally, by using the PPE technique in its front detection configuration,[37] the thermal effusivity at room temperature has been obtained for all the materials except for $Tb_2Dy_4FeSb_2$, due to the thickness limitations in this compound. Using the densities of each compound the specific heat capacity and thermal conductivity values have been obtained and are shown in Table 4. All the values are very close to each other within a small range.

4. Conclusions

Nine selected compounds of the R_6TX_2 (R = Gd, Tb, Dy; T = Mn, Fe, Co, Ni; X = Sb, Te) intermetallic family have been studied in detail. These compounds were selected based on previous studies of this family[29–31] in order to optimize their magnetocaloric performance and increase their working temperature up to room temperature, or close to it. As observed by magnetic measurements, two magnetic phase transitions take place in these materials. They have a ferromagnetic ordering below T_C (182–282 K) and a spin reorientation transition at a lower temperature, T_m = 26–76 K. This makes these materials suitable to work as magnetic refrigerators in both the room temperature region and the gas liquefaction region. The effect of the substitution of different atoms in the composition on T_C has been addressed. The increase of the rare earth atomic radius enlarges the atomic cell volume and *a* cell parameter, resulting in an increase of the Curie temperature. Regarding the effect of substituting the transition metal element, the strongest effect on T_C is observed with Mn, which greatly increases the PM–FM transition temperature. This element has the largest atomic radius among the transition metal elements studied in this work, and causes a big enlargement of the *c* cell parameter and cell volume, with a small shortening of the *a* cell parameter in comparison with Fe, Ni or Co. A stronger hybridization of Mn with the other elements of the compounds is also proposed in order to explain its impact on T_C. Three clear trends for the increase of the Curie temperature with the enlargement of the *c* cell parameter have been observed, depending on the rare earth element, transition metal and p-block element.

As observed in the magnetic entropy change data, the overlap of both transitions generates two peaks with a plateau region in between, without the need for using a composite material for this purpose. This table-like effect is required in order to improve the Ericsson cycle efficiency. Relevant magnetocaloric properties are found for the presented compounds, especially for $Tb_2Dy_4FeSb_2$, with $|\Delta S_M^{pk}|$ = 7.72 J kg^{-1} K^{-1} around 182 K for $\mu_0\Delta H$ = 5 T, and also for materials with T_C values closer to room temperature (233–282 K), for which $|\Delta S_M^{pk}|(\mu_0\Delta H = 5\ T)$ = 2.88–4.53 J kg^{-1} K^{-1}. Furthermore, having two consecutive magnetic phase transitions enhances the refrigerant capacity values, enlarging the temperature span of applicability of these compounds. This work has managed to show that the magnetocaloric performance can be improved and T_C can be displaced closer to room temperature by correctly tuning the composition. The thermal properties of the compounds have also been studied in order to establish their potential use as magnetic refrigerants. The photopyroelectric calorimetry measurements yield interesting and promising thermal diffusivity values. These results suggest that the compounds studied in this work may be suitable to work under high frequency refrigeration cycles. The critical behavior analysis of PM–FM transitions shows that besides $Tb_2Dy_4FeSb_2$, which unequivocally belongs to a Mean Field universality class, the remaining compounds do not match any theoretical model, presenting higher β values (0.59–0.90) than the ones corresponding to the known universality classes. These deviations are common in this R_6TX_2 intermetallic family, and point to the necessity of developing new theoretical models addressing more complex magnetic interactions that can explain the experimentally observed deviations. The obtained critical exponents have been used to successfully check the magnetocaloric scaling relations of the magnetic entropy change and refrigerant capacities. It has been discussed and proven that, when two magnetic phase transitions overlap, RC scaling can only be done if the peaks are considered symmetric. The collapse of the magnetic entropy change curves into a single universal or master curve has also been observed, confirming the second order nature of the PM–FM transition. Combining the scaling laws, critical exponents and universality curves allows the extrapolation of magnetic entropy curves to magnetic fields which are not experimentally accessible.[59]

Conflicts of interest

The authors declare that they have no known competing financial interests or personal relationships that could have appeared to influence the work reported in this paper.

Acknowledgements

This work was supported by Departamento de Educación del Gobierno Vasco (project IT1430-22) and the Russian Fund for Basic Research through the project no. 20-03-00209-a, as well as by an ICDD (International Centre for Diffraction Data) (USA) grant n 05-07. The unit cell data of $Gd_3Tb_3FeSbTe$ and $Tb_6Fe_{0.75}Mn_{0.25}SbTe$ were used with permission from – © JCPDS – International Centre for Diffraction Data. The authors are thankful for the technical and human support provided by SGIker (UPV/EHU/ERDF, EU).

References

1 V. Franco, J. S. Blázquez, J. J. Ipus, J. Y. Law, L. M. Moreno-Ramírez and A. Conde, Magnetocaloric effect: From materials research to refrigeration devices, *Prog. Mater. Sci.*, 2018, **93**, 112–232.
2 T. Gotschall, K. P. Skokov, M. Fries, A. Taubel, I. Radulov, F. Scheibel, D. Benke, S. Riegg and O. Gutfleisch, Making a

cool choice: the materials library of magnetic refrigeration, *Adv. Energy Mater.*, 2019, **9**(113), 1901322.

3 O. Gutfleisch, M. A. Willard, E. Brück, C. H. Chen, S. G. Sankar and J. P. Liu, Magnetic materials and devices for the 21st century: stronger, lighter, and more energy efficient, *Adv. Mater.*, 2011, **23**, 821–842.

4 N. K. Singha, K. G. Suresha, A. K. Nigamb, S. K. Malikb, A. A. Coelhoc and S. Gama, Itinerant electron metamagnetism and magnetocaloric effect in RCo2-based Laves phase compounds, *J. Magn. Magn. Mater.*, 2007, **317**, 68–79.

5 I. Tereshina, J. Cwik, E. Tereshina, G. Politova, G. Burkhanov, V. Chzhan, A. Ilyushin, M. Miller, A. Zaleski, K. Nenkov and L. Schultz, Multifunctional Phenomena in Rare-Earth IntermetallicCompounds With a Laves Phase Structure: Giant Magnetostriction and Magnetocaloric Effect, *IEEE Trans. Magn.*, 2014, **50**, 2504604.

6 V. Paul-Boncour, A. Herrero, V. Shtender, K. Provost and E. Elkaim, Magnetic transitions with magnetocaloric effects near room temperature related to structural transitions in Y0.9Pr0.1Fe2D3.5 deuteride, *J. Appl. Phys.*, 2021, **130**, 113904.

7 S. Gupta and K. G. Suresh, Review on magnetic and related properties of RTX compounds, *J. Alloys Compd.*, 2015, **618**, 562–606.

8 H. Zhang, Y. J. Sun, E. Niu, L. H. Yang, J. Shen, F. X. Hu, J. R. Sun and B. G. Shen, Large magnetocaloric effects of RFeSi (R = Tb and Dy) compounds for magnetic refrigeration in nitrogen and natural gas liquefaction, *Appl. Phys. Lett.*, 2013, **103**, 202412.

9 Y. Zhang, Review of the structural, magnetic and magnetocaloric properties in ternary rare earth RE_2T_2X type intermetallic compounds, *J. Alloys Compd.*, 2019, **787**, 1173–1186.

10 S. K. Tripathy, K. G. Suresh and A. K. Nigam, A comparative study of the magnetocaloric effect in Gd_3Co and Gd_3Ni, *J. Magn. Magn. Mater.*, 2006, **306**, 24–29.

11 B. Li, J. Du, W. J. Ren, W. J. Hu, Q. Zhang, D. Li and Z. D. Zhang, Large reversible magnetocaloric effect in Tb3Co compound, *Appl. Phys. Lett.*, 2008, **92**, 242504.

12 H. Zhang, R. Gimaev, B. Kovalev, K. Kamilov and V. Zverev, Review on the materials and devices for magnetic refrigeration in the temperature range of nitrogen and hydrogen liquefaction, *Physica B: Condens. Matter*, 2019, **558**, 65–73.

13 N. Raghu Ram, M. Prakash, U. Naresh, N. Suresh Kumar, T. Sofi Sarmash, T. Subbarao, R. Jeevan Kumar, G. Ranjith Kumar and K. Chandra Babu Naidu, Review on Magnetocaloric Effect and Materials, *J. Supercond. Novel Magn.*, 2018, **31**, 1971–1979.

14 M. Balli, S. Jandl, P. Fournier and A. Kedous-Lebouc, Advanced materials for magnetic cooling: Fundamentals and practical aspects, *Appl. Phys. Rev.*, 2017, **4**, 021305.

15 V. Franco, J. S. Blázquez, B. Ingale and A. Conde, The magnetocaloric effect and magnetic refrigeration near room temperature: Materials and Models, *Annu. Rev. Mater. Res.*, 2012, **42**, 305–342.

16 O. Gutfleisch, M. A. Willard, E. Brück, C. H. Chen, S. G. Sankar and J. P. Liu, Magnetic Materials and Devices for the 21st Century: Stronger, Lighter, and More Energy Efficient, *Adv. Mater.*, 2011, **23**, 821–842.

17 J. Y. Law, A. Diaz-Garcia, L. M. Moreno-Ramirez and V. Franco, Increased magnetocaloric response of FeMnNiGeSi high-entropy alloys, *Acta Mater.*, 2021, **212**, 116931.

18 J. Y. Law, L. M. Moreno-Ramirez, A. Diaz-Garcia, A. Martin-Cid, S. Kobayashi, S. Kawaguchi, T. Nakamura and V. Franco, MnFeNiGeSi high-entropy alloy with large magnetocaloric effect, *J. Alloys Compd.*, 2021, **855**, 157424.

19 V. Chaudhary, X. Chen and R. V. Ramanujan, Iron and manganese based magnetocaloric materials for near room temperature thermal management, *Prog. Mater. Sci.*, 2019, **100**, 64–98.

20 V. I. Zverev and A. M. Tishin, Magnetocaloric effect: from theory to practice, *Phys. Rep.*, 2010, **489**, 89–15.

21 L. Li and M. Yan, Recent progresses in exploring the rare earth based intermetallic compounds for cryogenic magnetic refrigeration, *J. Alloys Compd.*, 2020, **823**, 153810.

22 L. W. Li, Review of magnetic properties and magnetocaloric effect in the intermetallic compounds of rare earth with low boiling point metals, *Chin. Phys. B*, 2016, **25**, 037502.

23 H. Zhang, R. Gimaev, B. Kovalev, K. Kamilov and V. Zverev, Review on the materials and devices for magnetic refrigeration in the temperature range of nitrogen and hydrogen liquefaction, *Physica B: Condens. Matter*, 2019, **558**, 65–73.

24 A. M. Tishin, Y. I. Spichkin, V. I. Zverev and P. W. Egolf, A review and new perspectives for the magnetocaloric effect: New materials and local heating and cooling inside the human body, *Int. J. Refrig.*, 2016, **68**, 177–186.

25 A. M. Tishin and Y. I. Spichkin, *The Magnetocaloric Effect and its Applications, Series in Condensed Matter Physics*, Institute of Physics Publishing, Bristol and Philadelphia, 2003.

26 J. Romero-Gómez, R. Ferreriro-Garcia, A. De Miguel-Catoira and M. Romero-Gomez, Magnetocaloric effect: A review of the thermodynamic cycles in magnetic refrigeration, *Renewable Sustainable Energy Rev.*, 2013, **17**, 74–84.

27 O. Gutfleisch, T. Gottschall, M. Fries, D. Benke, I. Radulov, K. P. Skolov, H. Wende, M. Gruner, M. Acet, P. Entel and M. Farle, Mastering hysteresis in magnetocaloric materials, *Philos. Trans. R. Soc., A*, 2016, **374**, 20150308.

28 C. Jiang, J. Yan, X. Wang, S. Wei, P. Liang, Y. Chen, Y. Song and G. Han, Table-like magnetocaloric effect around room temperature of atiperovskite composite materials based on Mn3Sn1-XGaXC, *Mater. Today Commun.*, 2021, **27**, 102379.

29 A. Herrero, A. Oleaga, A. Salazar, A. V. Garshev, V. O. Yapaskurt and A. V. Morozkin, Magnetocaloric properties, magnetic interactions and critical behavior in $Ho_6(Fe,Mn)Bi_2$ intermetallics, *J. Alloys Compd.*, 2020, **821**, 153198.

30 A. Oleaga, A. Herrero, A. Salazar, A. V. Garshev, V. O. Yapaskurt and A. V. Morozkin, Magnetocaloric properties and unconventional critical behavior in (Gd,

Tb)$_6$(Fe,Mn)Bi$_2$ intermetallics, *J. Alloys Compd.*, 2020, **843**, 155937.

31 A. Herrero, A. Oleaga, I. R. Aseguinolaza, A. J. Garcia-Adeva, E. Apiñaniz, A. V. Garshev, V. O. Yapaskurt and A. V. Morozkin, Tailoring the magnetocaloric, magnetic and thermal properties of Dy$_6$(Fe,Mn)X$_2$ intermetallics (X=Sb, Te, Bi), *J. Alloys Compd.*, 2022, **890**, 161849.

32 *The Rietveld Method*, ed. F. Izumi and R. A. Young, Oxford University Press, Oxford, 1993, ch. 13.

33 H. Neves Bez, H. Yibole, A. Pathak, Y. Mudryk and V. K. Pecharsky, Best practices in evaluation of the magnetocaloric effect from bulk magnetization measurements, *J. Magn. Magn. Mater.*, 2018, **458**, 301–309.

34 W. Jiang, X. Z. Zhou, G. Williams, Y. Mukovskii and K. Glazyrin, Magnetic ground state and two-dimensional behavior in pseudo-kagome layered system Cu$_3$Bi(SeO$_3$)$_2$O$_2$Br, *Phys. Rev. B: Condens. Matter Mater. Phys.*, 2008, **78**, 144409.

35 W. Jiang, X. Z. Zhou, G. Williams, Y. Mukovskii and K. Glazyrin, Coexistence of colossal magnetoresistance, a Griffiths-like phase, and a ferromagnetic insulating ground state in single crystal La$_{0.73}$Ba$_{0.27}$MnO$_3$, *Phys. Rev. B: Condens. Matter Mater. Phys.*, 2008, **77**, 064424.

36 A. Oleaga, A. Salazar, D. Prabhakaran, J. G. Cheng and J. S. Zhou, Critical behavior of the paramagnetic to antiferromagnetic transition in orthorhombic and hexagonal phases of RMnO$_3$ (R = Sm, Tb, Dy, Ho, Er, Tm, Yb, Lu, Y), *Phys. Rev. B: Condens. Matter Mater. Phys.*, 2012, **85**, 184425.

37 U. Zammit, M. Marinelli, F. Mercuri, S. Paoloni and F. Scudieri, Invited review article: Photopyroelectric calorimenter for the simultaneous thermal, optical, and structural characterization of samples over phase transitions, *Rev. Sci. Instrum.*, 2011, **82**, 121101.

38 Springer Materials The Landolt-Börnstein Database – Materials Science Data for 250000 Substances, **https://www.springermaterials.com**.

39 J. Emsley, in *The elements*, Clarendon press, Oxford, 2nd edn, 1991; *Fizicheskie velichiny (Physical Data). Handbook*, ed. I. S. Grigor'ev and E. Z. Meilohov, Energoatomizdat, Moscow, 1994 (In Russian).

40 A. V. Morozkin, R. Nirmala and S. K. Malik, Structural and magnetic properties of Fe$_2$P-type R$_6$TX$_2$ compounds (R = Zr, Dy, Ho, Er, Tj Mn, Fe, Co, Cu, Ru, Rh, X = Sb, Bi, Te), *Intermetallics*, 2011, **19**, 1250–1264.

41 A. V. Morozkin, Y. Mozharivskyj, V. Svitlyk, R. Nirmala, O. Isnard, P. Manfrinetti, A. Provino and C. Ritter, Magnetic properties of Fe$_2$P-type R$_6$CoTe$_2$ compounds (R=Gd–Er), *J. Solid State Chem.*, 2010, **183**, 1314–1325.

42 A. V. Morozkin, V. N. Nikiforov and B. Malaman, Magnetic structure of the Zr$_6$CoAs$_2$- type Tb$_6$FeBi$_2$ compound, *J. Alloys Compd.*, 2005, **393**, L6–L9.

43 A. V. Morozkin, O. Isnard, P. Manfrinetti, A. Provino, C. Ritter, R. Nirmala and S. K. Malik, The magnetic ordering in the Ho$_6$FeTe$_2$, *J. Alloys Compd.*, 2010, **498**, 13–18.

44 J. Zhang, G. Shan, Z. Zheng and C. H. Shek, Structure and magnetic behaviors of Gd$_6$FeBi$_2$ compound, *Intermetallics*, 2016, **68**, 51–56.

45 J. Zhang, Y. M. Kang, G. Shan and S. Bobev, Structural analysis of Gd$_6$FeBi$_2$ from single-crystal X-ray diffraction methods and electronic structure calculations, *Acta Crystallogr., Sect. C: Struct. Chem.*, 2019, **75**, 562–567.

46 A. V. Morozkin, R. Nirmala and S. K. Malik, Magnetic structure of the Zr$_6$CoAs$_2$-type Er$_6$TX$_2$ compounds (T = Mn, Fe, Co and X = Sb, Bi), *J. Alloys Compd.*, 2005, **394**, 75–79.

47 A. V. Morozkin, Y. Mozharivskyj, V. Svitlyk, R. Nirmala and A. K. Nigam, Magnetic properties of Fe$_2$P-type Tb$_6$FeTe$_2$, Tb$_6$CoTe$_2$, Tb$_6$NiTe$_2$ and Er$_6$FeTe$_2$ compounds, *J. Solid State Chem.*, 2010, **183**, 3039–3051.

48 H. E. Stanley, *Introduction to phase transitions and critical phenomena*, Oxford University Press, 1971.

49 M. Campostrini, M. Hasenbusch, A. Pelissetto, P. Rossi and E. Vicari, 25th-order high- temperature expansion results for three-dimensional Ising-like systems on the simple-cubic lattice, *Phys. Rev. E: Stat., Nonlinear, Soft Matter Phys.*, 2002, **65**, 066127.

50 M. Campostrini, A. Pelisseto, P. Rossi and E. Vicari, 25-th order high-temperature expansion results for three-dimensional Ising-like systems on the simple-cubic lattice, *Phys. Rev. E: Stat., Nonlinear, Soft Matter Phys.*, 2002, **65**, 066127.

51 M. E. Fisher, S. K. Ma and B. G. Nickel, Critical exponents for long-range order interactions, *Phys. Rev. Lett.*, 1972, **29**, 917–920.

52 M. Campostrini, M. Hasenbusch, A. Pelisseto, P. Rossi and E. Vicari, Critical behavior of the three-dimensional XY universality class, *Phys. Rev. B: Condens. Matter Mater. Phys.*, 2001, **63**, 214503.

53 H. Kawamura, Universality of phase transitions of frustrated antiferromagnets, *J. Phys.: Condens. Matter*, 1998, **10**, 4707.

54 E. K. Riedel and F. J. Wegner, Tricritical Exponents and Scaling Fields, *Phys. Rev. Lett.*, 1972, **29**, 349–352.

55 J. C. LeGuillou and J. Zinn-Justin, Critical exponents from field theory, *Phys. Rev. B: Condens. Matter Mater. Phys.*, 1980, **221**, 3976–3998.

56 Y. Liu and C. Petrovic, Critical behavior of the quasi-two-dimensional weak itinerant ferromagnet trigonal chromium telluride Cr0.62Te, *Phys. Rev. B*, 2017, **96**, 134410.

57 A. T. Ogielski, Dynamics of three-dimensional Ising spin glasses in thermal equilibrium, *Phys. Rev. B: Condens. Matter Mater. Phys.*, 1985, **32**, 7384–7398.

58 L. D. Griffith, Y. Mudryk, J. Slaughter and V. K. Pecharsky, Material-based figure of merit for caloric materials, *J. Appl. Phys.*, 2018, **123**, 034902.

59 V. Franco, A. Conde, J. M. Romero-Enrique and J. S. Blázquez, A universal curve for the magnetocaloric effect: an analysis based on scaling relations, *J. Phys.: Condens. Matter*, 2008, **20**, 285207.

60 S. Fujieda, Y. Hasegawa, A. Fujita and K. Fukamichi, Thermal transport properties of magnetic

refrigerants La(FexSi1-x)13 and their hydrides, and $Gd_5Si_2Ge_2$ and MnAs, *J. Appl. Phys.*, 2004, **95**, 2429–2431.

61 A. Salazar, On thermal diffusivity, *Eur. J. Phys.*, 2003, **24**, 351–358.

62 H. S. Carslaw and J. C. Jaeger, *Conduction of Heat in Solids*, Oxford University Press, 1959.

63 D. Dadarlat, C. Tripon, I. R. White and D. Korte, Photopyroelectric spectroscopy and calorimetry, *J. Appl. Phys.*, 2022, **132**, 191101.